Soil Dynamics and Earthquake Engineering 131 (2020) 106042

Contents lists available at ScienceDirect

Soil Dynamics and Earthquake Engineering

journal homepage: http://www.elsevier.com/locate/soildyn

A continuous-discrete approach for pre-design of flexible-base tall buildings with fluid viscous dampers

Iván F. Huergo [a], Hugo Hernández-Barrios [a,b,*], Carlos M. Patlán [b]

[a] School of Engineering, Universidad Nacional Autónoma de México, Mexico City, Mexico
[b] School of Engineering, Universidad Michoacana de San Nicolás de Hidalgo, Morelia, Mexico

ARTICLE INFO

Keywords:
Coupled-two beam model
Earthquake engineering
Fluid viscous dampers
Soil-structure interaction
Tall buildings
Wind engineering

ABSTRACT

An equivalent coupled-two-beam (CTB) discrete model is presented to compute the dynamic response in time domain of flexible-base buildings with linear fluid viscous dampers (FVDs). The equivalent model consists of a flexural cantilever beam and a shear cantilever beam connected in parallel by a finite number of axially rigid members that allows the consideration of intermediate modes of lateral deformation. The effects of different lateral deformations on the pre-design stage of two high-rise buildings are showed considering four soil types (hard rock, dense soil, stiff soil and soft soil) and three different distribution methods for linear FVDs: uniform-distribution (UD), story-shear-proportional-distribution (SSPD) and story-shear-strain-energy-distribution (SSSED). For UD method, the damping coefficients of FVDs increase as the flexural rigidity of the building decreases; whereas for SSPD and SSSED methods, the damping coefficients of FVDs vary along the height depending on the type of lateral deformation. For the three distribution methods and the same lateral deformation, the damping coefficients of FVDs decrease as the soil flexibility increases, which leads to a significant decrease in controlling earthquake-induced vibrations and wind-induced vibrations in the two high-rise buildings on a soft soil.

1. Introduction

Increasing urbanisation in recent decades has led to the construction of high-rise buildings worldwide, which are susceptible to seismic and wind loads. Currently, the structural design of tall buildings must satisfy different criteria such as strength, ductility, stability, resilience, sustainability, among others. Earthquake engineering is usually governed by the ultimate limit state, where peak displacements are of great importance to avoid damage in the structure. On the other hand, wind engineering is usually governed by the serviceability limit state, where root-mean-square (RMS) accelerations are of great importance to avoid human discomfort. The lateral deformation of buildings strongly depends on the type of lateral resisting system, which is usually depends on the height of the building. Accordingly, low-rise buildings usually deform like pure shear beams; whereas in medium-rise and high-rise buildings, the flexural deformation is as significant as the shear deformation.

Simplified continuous models are one of the most used procedures for pre-design complex structures and performing parametric analyses to identify the most important variables during the design process. The continuous Timoshenko beam [1] reflects a series coupling of the beam's bending and shear stiffnesses, while the coupled-two-beam (CTB) continuous model [2] couples the bending and shear stiffnesses in parallel. Dym and Williams [3] concluded that a series coupling of both stiffnesses do not display the correct dependence of frequency on building height, particularly in shear wall-frame buildings and tube-and-core constructions with the parallel nature of the two-beam model in which transverse displacements due to bending and to shear are identical. In conclusion, it appears that the CTB model seems the better model for estimating the frequencies of tall buildings because it provides predictions that are consistent with the observed data [3].

The CTB continuous model [2] has a fixed base, therefore, it is not applicable in those buildings where the soil-structure interaction (SSI) is important due to the parameters of the soil and the foundation. Cruz and Miranda [4,5] evaluated the effects of SSI on damping ratios of buildings subjected to earthquake ground motions through an equivalent fixed-base multistory model; however, they do not incorporate a flexible base in the CTB continuous model [2]. Wu, Zhao and Lu [6]

* Corresponding author. School of Engineering, Universidad Michoacana de San Nicolás de Hidalgo, Morelia, Mexico.
E-mail address: hugohernandezbarrios@gmail.com (H. Hernández-Barrios).

https://doi.org/10.1016/j.soildyn.2020.106042
Received 13 November 2019; Received in revised form 11 January 2020; Accepted 14 January 2020
Available online 23 January 2020

incorporated a rotational spring at the base of the CTB continuous model [2], however, this extended CTB model does not contemplate the other parameters of the foundation (mass, mass moment of inertia, translational spring stiffness, translational damping coefficient and rotational damping coefficient). Huergo and Hernández [7] developed a discrete model equivalent to the CTB continuous model [2], which subsequently allowed the incorporation of SSI to the CTB model [8].

Passive energy dissipation devices offer an effective alternative for controlling the dynamic lateral response of tall buildings, a particular case of these devices are FVDs. FVDs are hydraulic cylinder-shaped devices that dissipate the kinetic energy of seismic events and wind loads through the reaction force of a compressible silicone fluid that flows through a valve system inside the device. The use of FVDs has gained popularity in the last few decades, mainly due to the large energy dissipation capability, the generation of forces that are out of phase with displacements and the possibility of increasing the damping ratio of a structure without significantly altering the inherent stiffness characteristics [9]. Manufactured FVDs that are used in buildings can produce forces that vary linearly with the relative velocities between the ends of the dampers. However, to provide more design freedom, damper manufacturers often produce dampers that can induce a force that is a nonlinear function of the relative velocity at the ends of the damper. Structural analysis of buildings equipped with nonlinear FVDs can be performed by the consideration of equivalent linear damping coefficients computed through linearization procedures [10–14]; however, for pre-design purposes, the nonlinear behavior of FVDs can be neglected [15].

Xu, He and Ko [16] performed an extensive parametric study to find optimum damper properties for adjacent buildings of different stiffness ratios and different heights, while Patel and Jangid [17] performed a similar parametric study for identical adjacent structures. However, the used formulation in both studies is only applicable for adjacent buildings that deform like pure shear beams.

Rama et al. [18] and Halperin et al. [19] developed methodologies to improve the seismic performance of buildings with FVDs, however, both studies do not contemplate intermediate modes of lateral deformation, neither SSI.

Apostolakis and Dargush [20] proposed a computational framework for the optimal distribution and design of yielding metallic buckling restrained braces and/or friction dampers within steel moment-resisting frames, which could be applied to other passive dissipation systems such as FVDs. On the other hand, the distribution of FVDs among different bays may be of crucial importance in view of the increase of axial loads induced by FVDs that may cause overstressing of columns [9].

Several studies [21–26] focus on active structural control of buildings including SSI, which show that the ratio of the fundamental natural period of the structure to that of the surface ground is a key parameter for characterizing the optimal placement of FVDs. However, all these studies [21–26] were based on multi-degree-of-freedom (MDOF) shear building models.

For designing a building structure with supplemental linear FVDs, the damping coefficient of the dampers can be easily determined corresponding to a desired added damping ratio and the fundamental dynamic properties such as the vibration mode shape and natural period of a structure. The formulas commonly used to calculate the supplementary damping of the FVDs are those proposed by FEMA 273/274 and FEMA 356 [27],however, the relative vertical deformation between the ends of the FVD was not considered when such formulas were derived. This has resulted into the lack of accuracy for predicting the added damping ratio of medium-rise to high-rise buildings, where the flexural deformation is as significant as the shear deformation. To solve that problem, Hwang et al. [28] developed new design formulas for FVDs that take into account the relative vertical and horizontal deformation between the two ends of a viscous damper so that the axial deformation of the damper and thus the dissipated energy by the damper can be better captured for medium-rise and high-rise buildings.

Hwang et al. [29] compared various methods for distributing damping coefficients of FVDs along the height of three planar frames with fixed base. Motivated by the concept of composite damping ratio weighted by the element strain energy, Hwang et al. [29] proposed to distribute the FVDs in proportion to the storey shear strain energy, concluding that this method may provide the better choices for the practical design of FVDs.

De Domenico, Ricciardi and Takewaki [9] presented an overview of the most popular methodologies from the abundant literature for design of FVDs for seismic protection of buildings structures, focusing on the optimal damping coefficients and the optimal placement of FVDs. This study demonstrates that existing methodologies for design of FVDs do not contemplate intermediate modes of lateral deformation and SSI because they are also based on MDOF shear buildings models with fixed base, in spite of the notorious dependence of distribution methods [29] on the fundamental period and its associated mode shape.

FVDs have been extensively studied through fixed-base MDOF shear buildings models [9–19,29], on the contrary, these passive energy dissipation devices have been little studied through flexible-base MDOF shear buildings models [21–26]. However, these simplified models [9–26,29] do not contemplate intermediate modes of lateral deformation despite the added damping provided by FVDs depend directly on the lateral deformation of the building [28,29]. In this paper, linear FVDs are incorporated to the flexible-base CTB model [8] in order to evaluate the effects of different lateral deformations and SSI on three distribution methods for FVDs: uniform-distribution (UD), story-shear-proportional-distribution (SSPD) and story-shear-strain -energy-distribution (SSSED).

2. Flexible-base CTB model with FVDs

A flexible-base N-story tall building with different brace configurations of FVDs can be schematically represented as shown in Fig. 1.

Fig. 1 reflects a parallel coupling of the building's bending and shear stiffnesses. The shear wall (bending deflection) and rigid frame (shear deformation) are connected in parallel by a finite number of axially rigid members that allows the consideration of intermediate modes of lateral deformation. The lateral relative displacement of the jth story of the building is defined as $u_j(t)$, where j=1,2,3,…,N. The foundation of the building rests on an elastic half-space, where p_s, V_s and v_s are defined, respectively as soil density, shear-wave velocity of soil and soil Poisson's ratio. In addition, $c_{d,j}(j=1,2,3,\ldots,N)$ and $f_j(j=1,2,3,\ldots,N)$ represent respectively the damping coefficient and magnification factor of the jth FVD. Values of $f_j(j=1,2,3,\ldots,N)$ for some common brace configurations [30–33] are depicted in Fig. 1.

Experiments carried out on FVDs have revealed that the damper force can reasonably be considered proportional to the relative velocity between the ends of the device [34]. According to the sketch in Fig. 1, the FVD force at the jth story is

$$f_{d,j} = c_{d,j}\left|\Delta\dot{w}_j\right|^{\eta_j}\operatorname{sgn}\left(\Delta\dot{w}_j\right) \tag{1}$$

where $c_{d,j}$ $(j=1,2,3,\ldots,N)$ and $\eta_j(j=1,2,3,\ldots,N)$ represent the damping coefficient and power law exponent of the jth FVD, respectively, and $\Delta\dot{w}_j$ is the relative velocity at the ends of the jth FVD, which may be different from the interstory velocity at the jth story $\Delta\dot{u}_j = \dot{u}_j - \dot{u}_{j-1}$. In a general way, the value of $\Delta\dot{w}_j$is related to the interstory velocity through the magnification factorf_j, that is, $\Delta\dot{w}_j = f_j\,\Delta\dot{u}_j$. Values of η_j are generally less than one, however, for a pre-design stage, it is usually assumed a linear behavior for the FVDs [15], that is, $\eta_j = 1$. Adopting a simplified linear model, the FVD force at the jth story is

$$f_{d,j} = c_{d,j}\,\Delta\dot{w}_j = c_{d,j} f_j\,\Delta\dot{u}_j \tag{2}$$

The linear forces exerted by the N FVDs may be expressed as

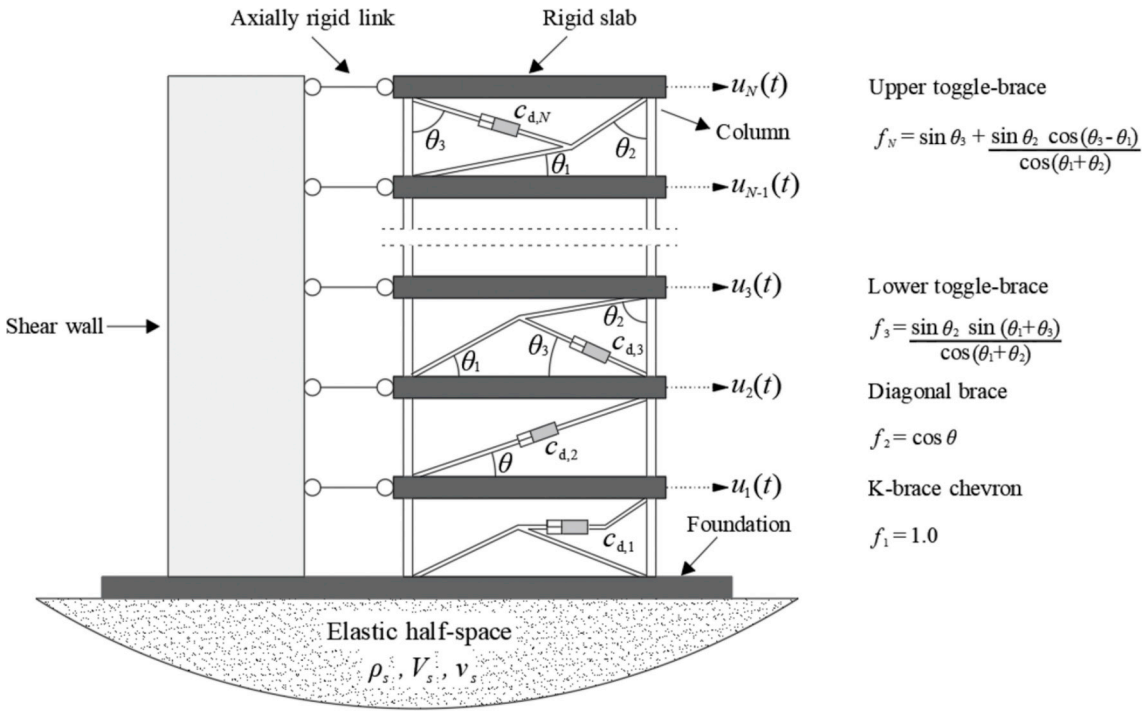

Fig. 1. Sketch of an *N*-story shear wall-frame building with FVDs including SSI.

$$\{f_{d,j}\}_{N\times 1} = [C_d]_{N\times N}\{\dot{u}(t)\}_{N\times 1} \tag{3}$$

where $\{\dot{u}(t)\}_{N\times 1}$ is a column vector containing the relative velocities of the stories and

$$[C_d]_{N\times N} = [R]^T[D][R] \tag{4}$$

For interstory dampers implemented at every story through common brace configurations (see Fig. 1), matrices $[R]$ and $[D]$ shown in Eq. (4) are given by Ref. [9].

$$[R] = \begin{bmatrix} f_1 & 0 & \dots & & & 0 \\ -f_2 & f_2 & 0 & \dots & & 0 \\ 0 & -f_3 & f_3 & 0 & \dots & 0 \\ \vdots & & & \ddots & & \vdots \\ 0 & \dots & 0 & -f_{N-1} & f_{N-1} & 0 \\ 0 & \dots & & 0 & -f_N & f_N \end{bmatrix} \tag{5}$$

$$[D] = \begin{bmatrix} c_{d,1} & & \\ & \ddots & \\ & & c_{d,N} \end{bmatrix} \tag{6}$$

For nonlinear FVDs ($\eta_j \neq 1$), equivalent linear damping coefficients for the FVDs can be computed through linearization procedures [10–14]; however, for pre-design purposes, the nonlinear behavior of FVDs can be neglected [15]. For linear FVDs ($\eta_j = 1$), the damping coefficients of the FVDs can be computed through some distribution methods [29]: uniform-distribution (UD), storey-shear-proportional-distribution (SSPD) and storey-shear-strain-energy-distribution (SSSED), among others.

The UD method assumes that the damping coefficients $c_{d,j}$ are identical at every storey and equal to

$$c_{d,j} = \frac{4\pi\xi_d}{T_1} \frac{\sum_{i=1}^{N} m_i \varphi_{1,i}^2}{\sum_{j=1}^{n_d} f_j^2 (\varphi_{1,j} - \varphi_{1,j-1})^2} \tag{7}$$

where n_d is the number of FVDs; ξ_d is the supplemental damping ratio contributed by the n_d FVDs, T_1 is the fundamental period of vibration of the flexible-base building, m_i (i=1,2,3,…,N) is the lumped mass at the ith story, φ_1 is the first eigenvector of the undamped flexible-base building and f_j is the magnification factor (see Fig. 1).

The SSPD method proposes to distribute the FVDs in proportion to the design story shears $V_{s,j}$, assuming that the value of $V_{s,j}$ at the storey j is proportional to the parameter $S_j = \sum_{i=j}^{N} m_i \varphi_{1,i}$. Accordingly, the damping coefficients $c_{d,j}$ are equal to

$$c_{d,j} = \frac{4\pi\xi_d}{T_1} \frac{S_j \sum_{i=1}^{N} m_i \varphi_{1,i}^2}{\sum_{j=1}^{n_d} S_j f_j^2 (\varphi_{1,j} - \varphi_{1,j-1})^2} \tag{8}$$

The SSSED method proposes to distribute the FVDs in proportion to the storey shear strain energy, which can be considered proportional to the parameter $\psi_j = S_j(\varphi_{1,j} - \varphi_{1,j-1})$, where S_j has already been introduced above. Accordingly, the damping coefficients $c_{d,j}$ are equal to

$$c_{d,j} = \frac{4\pi\xi_d}{T_1} \frac{\psi_j \sum_{i=1}^{N} m_i \varphi_{1,i}^2}{\sum_{j=1}^{n_d} \psi_j f_j^2 (\varphi_{1,j} - \varphi_{1,j-1})^2} \tag{9}$$

Hwang et al. [29] introduced an additional distribution method as a refinement of the SSSED, in which the dampers are distributed only in those storeys in which the strain energy exceeds the average strain energy, which was called storey-shear-strain-energy-to-efficient-storeys-distribution (SSSEESD). De Domenico et al. [9] demonstrated that added damping ratio and displacement profiles are comparable between SSSED and SSSEESD, however, for SSSEESD and a non-regular-in elevation structure, the response in terms of interstory drifts and absolute floor accelerations increases significantly for the higher stories wherein no dampers are installed. Only the UD, the SSPD and the SSSED are considered in this paper.

According to the classification presented by De Domenico, Ricciardi and Takewaki [9], the three distribution methods of linear FVDs used in

this paper belong to the heuristic class; therefore, they do not achieve an optimum response against any response indicator of the building, that is, the interstory drift ratio, the peak displacement, the absolute acceleration, among others.

Reasonable and economical values for added damping ratio ξ_d vary between 5-15%, introducing negligible influence on the fundamental natural period of the structure [28].

The lateral resisting system and SSI significantly modify the dynamic properties of the building (periods, mode shapes and damping), however, Eqs. (7)–(9) have only been used in fixed-base MDOF shear buildings models [9–19,29]. For this reason, a simplified discrete model of the sketch shown in Fig. 1 is developed in this paper (see Fig. 2), which is only valid for planar models, that is, the proposed model is not able to consider torsional effects.

The proposed model represents an N-story building with flexible base and n_d FVDs ($N = n_d$), which can be subjected to the horizontal ground acceleration $\ddot{u}_g(t)$ or to the wind forces $F(z,t)$. The proposed CTB model (see Fig. 2) consists of a flexural cantilever beam and a shear cantilever beam connected in parallel by a finite number of axially rigid members that allow the consideration of intermediate modes of lateral deformation. The total height of the building H is divided into N stories with length L_j(j=1,2,3,…,N); this means that each beam of the CTB model is divided into N finite elements. The jth node of the flexural cantilever beam is connected to the jth node of the shear cantilever beam by an axially rigid member denoted as $k_j^a \to \infty$ (j=1,2,3,…,N), which allows the coupling between both beams. m_0 and I_0 are defined, respectively as mass and mass moment of inertia of the foundation. k_t and k_θ are defined, respectively as the translational spring stiffness and rotational spring stiffness of the foundation. c_t and c_θ are defined, respectively as the translational damping coefficient and rotational damping coefficient of the foundation. In addition, $c_{d,j}$ (j=1,2,3,…,N) is the damping coefficient of the jth FVD for any of common brace configurations shown in Fig. 1.

Literature features refined models of soil that contemplate various effects such as the nonlinearity of soil behavior [35–37], however, for practical engineering purposes, the soil model adopted in this paper is the simplest one, which is based on static foundation stiffnesses. Kausel [38] developed a concise review of the state of art of such static solutions. Under these assumptions and considering a rigid circular foundation, the coefficients of the springs and dashpots for the translational and rotational motions of the foundation are computed using the following formulas [39]:

$$k_t = \frac{8 G_s r_0}{2 - \nu_s} \tag{10}$$

$$k_\theta = \frac{8 G_s r_0^3}{3(1 - \nu_s)} \tag{11}$$

$$c_t = \frac{4.6 \rho_s V_s r_0^2}{2 - \nu_s} \tag{12}$$

$$c_\theta = \frac{0.4 \ \rho_s \ V_s \ r_0^4}{1 - \nu_s} \tag{13}$$

where

$$G_s = \frac{E_s}{2(1 + \nu_s)} \tag{14}$$

$$V_s = \sqrt{\frac{G_s}{\rho_s}} \tag{15}$$

In Eqs. 10–15, G_s is the shear modulus of soil, r_0 is the equivalent radius of the foundation, ν_s is the soil Poisson's ratio, ρ_s is the soil density, V_s is the shear-wave velocity of soil and E_s is the soil Young's modulus. Once these parameters are known, it is possible to determine the stiffness and damping matrices that represent the flexible base of the flexural beam and the shear beam, which are given by

$$[K_s^F] = [K_s^S] = \begin{bmatrix} \frac{k_\theta}{2} & \\ & \frac{k_t}{2} \end{bmatrix} \tag{16}$$

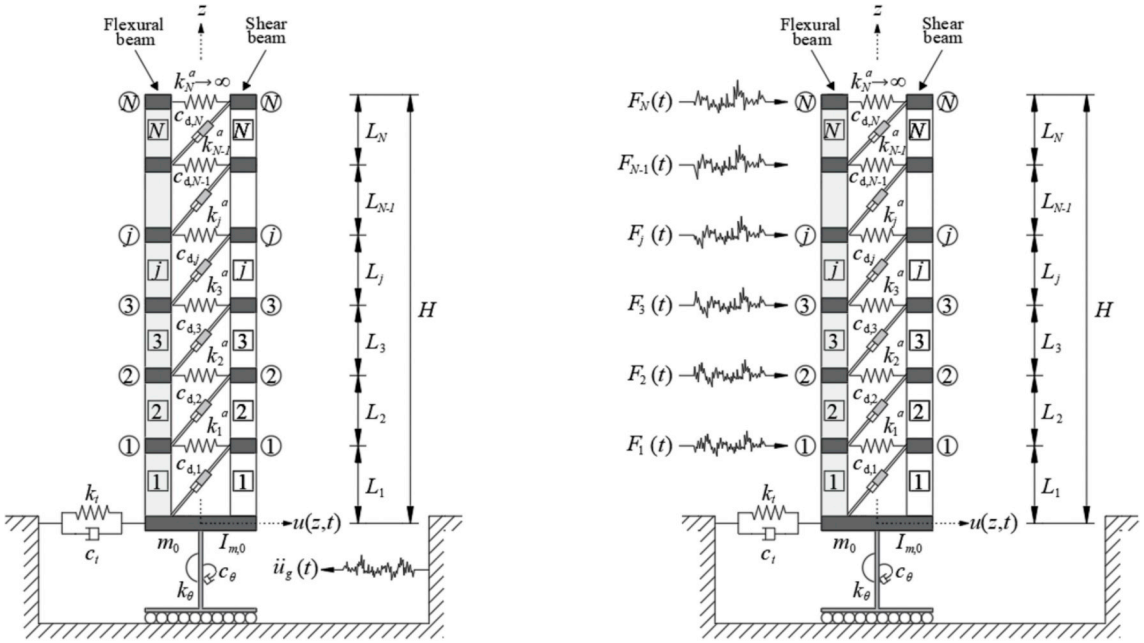

Fig. 2. CTB model for a flexible-base tall building with FVDs.

$$\left[C_s^F\right] = \left[C_s^S\right] = \begin{bmatrix} \frac{c_\theta}{2} & \\ & \frac{c_t}{2} \end{bmatrix} \tag{17}$$

where superscripts F and S are associated with the flexural beam and shear beam, respectively.

The flexible-base CTB model with FVDs (see Fig. 2) consists of $2N + 4$ equations of motion if it is considered that $N = n_d$. The equations can be grouped in a matrix system given by

$$[M_{CTB}]\ \{\ddot{u}_{CTB}(t)\} + [C_{CTB}]\ \{\dot{u}_{CTB}(t)\} + [K_{CTB}]\ \{u_{CTB}(t)\} = \{F_{CTB}(t)\} \tag{18}$$

The external forces of the building are divided into two proportional parts for each cantilever beam in such a way that

$$\{F_{CTB}(t)\} = \left[\ \left\{F_\Psi^F(t)\right\}\quad \left\{F_\Psi^S(t)\right\}\ \right]^T \tag{19}$$

where for seismic loads (see Fig. 2a)

$$\left\{F_\Psi^\lambda(t)\right\} = -\ddot{u}_g(t)\left\{\sum_{j=1}^{N} z_j\quad m_j^\lambda\quad \frac{m_0}{2} + \sum_{j=1}^{N} m_j^\lambda\quad \left\{m_j^\lambda\right\}_{1\times N}\right\} \tag{20}$$

assuming the superscript $\lambda = F = S$, m_j^F is the lumped mass at jth node of the flexural cantilever beam and m_j^S is the lumped mass at jth node of the shear cantilever beam. For wind loads (see Fig. 2b),

$$\left\{F_\Psi^F(t)\right\} = \left\{F_\Psi^S(t)\right\} = \left\{\sum_{j=1}^{N} \frac{z_j\ F_j(t)}{2}\quad \sum_{j=1}^{N} \frac{F_j(t)}{2}\quad \frac{1}{2}\left\{F_j(t)\right\}_{1\times N}\right\} \tag{21}$$

In equations (20) and (21), the external forces associated with each cantilever beam are composed of 3 subvectors: the overturning moment, the shear base force and the lateral external forces related to each story.

The displacements of the matrix equation (18) are given by

$$\{u_{CTB}(t)\} = \left[\ \left\{u_\Psi^F(t)\right\}\quad \left\{u_\Psi^S(t)\right\}\ \right]^T \tag{22}$$

where

$$\left\{u_\Psi^F(t)\right\} = \left\{u_\Psi^S(t)\right\} = \left\{\ \theta_0(t)\quad u_0(t)\quad \left\{u_j(t)\right\}_{1\times N}\ \right\} \tag{23}$$

In Eq. (23), $\theta_0(t)$ is the rotation of the foundation of the building, $u_0(t)$ is the lateral displacement of the foundation of the building, and $u_j(t)$ is the lateral relative displacement of the jth story of the building. The total displacement of the jth story of the building is given by

$$u_{\text{total},j}(t) = u_0(t) + z_j\ \ \theta_0(t)\ \ + u_j(t) \tag{24}$$

The mass matrix of the matrix equation (18) is given by

$$[M_{CTB}] = \begin{bmatrix} \left[M_\Psi^F\right] & [0]_{(N+2)\times(N+2)} \\ [0]_{(N+2)\times(N+2)} & \left[M_\Psi^S\right] \end{bmatrix} \tag{25}$$

The total mass of the building is divided into two proportional parts for each cantilever beam, in a similar way, the mass of each finite element of both beams (see Fig. 2) is divided into two proportional parts for each node. Considering these assumptions, the lumped mass matrix of the decoupled flexural beam, $[M_\Delta^F]_{N\times N}$, and the lumped mass matrix of the decoupled shear beam, $[M_\Delta^S]_{N\times N}$, are assembled. The jth elements of diagonal matrix $[M_\Delta^F]_{N\times N}$ and diagonal matrix $[M_\Delta^S]_{N\times N}$ are represented by $m_j^F (j=1,2,3,\ldots,N)$ and m_j^S $(j=1,2,3,\ldots,N)$, respectively; where $m_j^F + m_j^S$ represents the lumped mass at the jth story of the building. The submatrices of matrix $[M_{CTB}]$ shown in Eq. (25) are given by

$$\left[M_\Psi^\lambda\right] = \begin{bmatrix} \frac{I_{m,0}}{2} + \sum_{j=1}^{N}\left(\frac{I_{m,j}}{2} + m_j^\lambda z_j^2\right) & \sum_{j=1}^{N} m_j^\lambda z_j & \left\{m_j^\lambda z_j\right\}_{1\times N} \\ \sum_{j=1}^{N} m_j^\lambda z_j & \frac{m_0}{2} + \sum_{j=1}^{N} m_j^\lambda & \left\{m_j^\lambda\right\}_{1\times N} \\ \left\{m_j^\lambda z_j\right\}_{N\times 1} & \left\{m_j^\lambda\right\}_{N\times 1} & \left[M_\Delta^\lambda\right]_{N\times N} \end{bmatrix} \tag{26}$$

where $\lambda = F$ is referred to the flexural beam and $\lambda = S$ is referred to the shear beam; $I_{m,j}$ is the mass moment of inertia of the jth story of the building and z_j $(j=1,2,3,\ldots,N)$ is the height at jth node.

The stiffness matrix of the matrix equation (18) is given by

$$[K_{CTB}] = \begin{bmatrix} \left[K_\Psi^F\right] & \left[K_\Psi^C\right] \\ \left[K_\Psi^C\right] & \left[K_\Psi^S\right] \end{bmatrix} \tag{27}$$

where

$$\left[K_\Psi^\lambda\right] = \begin{bmatrix} \left[K_s^\lambda\right] & [0]_{2\times N} \\ [0]_{N\times 2} & \left[K_\Delta^\lambda\right]_{N\times N} + \left[K^A\right] \end{bmatrix} \tag{28}$$

$$\left[K_\Psi^C\right] = \begin{bmatrix} [0]_{2\times 2} & [0]_{2\times N} \\ [0]_{N\times 2} & -\left[K^A\right] \end{bmatrix} \tag{29}$$

the superscript $\lambda = F = S$, $[K_s^F]$ and $[K_s^S]$ are the soil's stiffness matrices defined in Eq. (16), $[K_\Delta^F]_{N\times N}$ is the condensed stiffness matrix of the decoupled flexural beam and $[K_\Delta^S]_{N\times N}$ is the condensed stiffness matrix of the decoupled shear beam. On the other hand, the axially rigid members (see Figs. 1-2) are assembled in a diagonal matrix given by

$$\left[K^A\right] = \begin{bmatrix} k_1^a \to \infty & & \\ & \ddots & \\ & & k_N^a \to \infty \end{bmatrix} \tag{30}$$

The condensed stiffness matrices $[K_\Delta^F]_{N\times N}$ and $[K_\Delta^S]_{N\times N}$ are defined once the global $2N \times 2N$ stiffness matrices of both decoupled beams are assembled, where the axial deformation is assumed to be negligible. For the jth finite element of each cantilever beam (see Fig. 2), the node j and the node $j+1$ are denoted as node A and node B, respectively. Neglecting axial deformation, each node of each cantilever beam has two degrees of freedom: a nodal displacement and a nodal rotation. Accordingly, the stiffness matrix of each finite element is composed by 4 submatrices $([K_{j,AA}], [K_{j,AB}], [K_{j,BA}], [K_{j,BB}])$, where each submatrix represents the forces applied in the first node (A or B) that generate unit displacements and unit rotations in the second node (A or B). Accordingly, the stiffness matrix of the jth finite element of the flexural cantilever beam (see Fig. 2) is given by

$$\left[K_{b,j}^F\right] = \begin{bmatrix} \left[K_{j,AA}^F\right] & \left[K_{j,AB}^F\right] \\ \left[K_{j,BA}^F\right] & \left[K_{j,BB}^F\right] \end{bmatrix} = \frac{EI}{L_j^3}\begin{bmatrix} \begin{bmatrix} 12 & 6L_j \\ 6L_j & 4L_j^2 \end{bmatrix} & \begin{bmatrix} -12 & 6L_j \\ -6L_j & 2L_j^2 \end{bmatrix} \\ \begin{bmatrix} -12 & -6L_j \\ 6L_j & 2L_j^2 \end{bmatrix} & \begin{bmatrix} 12 & -6L_j \\ -6L_j & 4L_j^2 \end{bmatrix} \end{bmatrix} \tag{31}$$

and the stiffness matrix of the jth finite element of the shear cantilever beam (see Fig. 2) is given by

$$\left[K^S_{b,j}\right]=\begin{bmatrix}\left[K^S_{j,AA}\right] & \left[K^S_{j,AB}\right]\\ \left[K^S_{j,BA}\right] & \left[K^S_{j,BB}\right]\end{bmatrix}=\frac{(EI)^S}{L_j^3(1+\delta)}\begin{bmatrix}\begin{bmatrix}12 & 6L_j\\ 6L_j & (4+\delta)L_j^2\end{bmatrix} & \begin{bmatrix}-12 & 6L_j\\ -6L_j & (2-\delta)L_j^2\end{bmatrix}\\ \begin{bmatrix}-12 & -6L_j\\ 6L_j & (2-\delta)L_j^2\end{bmatrix} & \begin{bmatrix}12 & -6L_j\\ -6L_j & (4+\delta)L_j^2\end{bmatrix}\end{bmatrix} \tag{32}$$

where $E\,I$ is the corresponding flexural rigidity of the jth story of the building, $(E\,I)^S$ is an equivalent flexural rigidity for the jth finite element of the shear cantilever beam (see Fig. 2) and δ is the non-dimensional stiffness parameter of a discrete Timoshenko beam. In equation (32), $(E\,I)^S\to\infty$, which means that the radius of gyration also tends to infinity, thus guaranteeing a pure shear deformation regardless of the slenderness ratio of the shear cantilever beam. If floor masses and lateral stiffnesses are assumed to remain constant along the height of the building, $E\,I$ and δ can be deduced through a mathematical adjustment [7,8] based on the CTB continuous model [2] as follows:

$$EI=\frac{4\overline{m}\;\;\pi^2\;H^4}{\left(T_1^*\gamma_1\right)^2\left(\gamma_1^2+\alpha^2\right)} \tag{33}$$

$$\delta=\frac{12\;(E\;I)^S}{G\;A^S\;L_j^2}=\frac{3\;(E\;I)^S\left(T_1^*\;\gamma_1\right)^2\left(\gamma_1^2+\alpha^2\right)}{\overline{m}\;\left(\pi\;\alpha\;H\;L_j\right)^2} \tag{34}$$

where $\overline{m}$ is the mass per unit length of the building; H is the total height of the building; L_j is the length of the jth finite element; T_1^* is the fundamental period of vibration of the fixed-base building, which can be computed by any of the existing empirical formulas [40–44]; $G\,A^S$ is the effective shear rigidity of the jth story of the building; $(E\,I)^S\to\infty$; and γ_1 is an eigenvalue parameter related to the first mode shape of the fixed-base CTB continuous model, that is, the first root of the following characteristic equation [2].

$$2+\left(2+\frac{\alpha^4}{\gamma_i^2\;(\alpha^2+\gamma_i^2)}\right)\cos(\gamma_i)\cosh\left(\sqrt{\alpha^2+\gamma_i^2}\right)+\left(\frac{\alpha^2}{\gamma_i\;\sqrt{\alpha^2+\gamma_i^2}}\right)\sin(\gamma_i)\sinh\left(\sqrt{\alpha^2+\gamma_i^2}\right)=0 \tag{35}$$

where i=1,2,3,…, ∞ and

$$\alpha=H\sqrt{\frac{G\,A^S}{E\,I}} \tag{36}$$

The parameter α is the non-dimensional lateral stiffness ratio that controls the degree of participation of overall flexural and overall shear deformations in the CTB model. A value of $\alpha\to0$ represents a pure flexural model (Euler–Bernoulli beam), whereas a value of $\alpha\to\infty$ represents a pure shear model. Miranda and Reyes [45] indicated that lateral deflected shapes of buildings whose lateral resisting system consists only of structural walls can usually be approximated by using values of α between 0 and 2. The same study indicated that for buildings with dual lateral resisting systems consisting of a combination of moment-resisting frames and shear walls or a combination of moment-resisting frames and braced frames, values of α are typically between 1.5 and 6; while for buildings whose lateral resisting system consists only of moment-resisting frames, values of α are typically between 5 and 20. Miranda and Reyes [45] also indicated that $\alpha=20$ represents a model very close to the pure shear model ($\alpha\to\infty$).

The stiffness matrices of each finite element (Eqs. (31)-(32)) are assembled by the conventional numerical assembly technique for the finite element method in order to obtain the global $2N\times2N$ stiffness matrices of the decoupled flexural and shear beams. It is necessary to perform a static condensation [46] of the $2N\times2N$ stiffness matrices in such a way that only translational degrees of freedom remain active. In this way, the condensed stiffness matrix of the decoupled flexural beam, $[K^F_\Delta]_{N\times N}$, and the condensed stiffness matrix of the decoupled shear beam, $[K^S_\Delta]_{N\times N}$, are obtained, which only depend on a few parameters: $\overline{m}$, H, T_1^*, γ_1 and α.

Rayleigh damping [46] is assumed for both decoupled beams (see Fig. 2). The damping matrix of the decoupled flexural beam and the damping matrix of the decoupled shear beam are represented by $[C^F_\Delta]_{N\times N}$ and $[C^S_\Delta]_{N\times N}$, respectively. Both matrices are computed with the prior knowledge of w_j^F, w_j^S, ξ_1 and ξ_2; where ξ_1 and ξ_2 are the modal damping ratios corresponding to the first and second mode of vibration of the fixed-base building in a particular translational direction. On the other hand, w_j^F(j = 1, 2, 3,…, N) and w_j^S (j = 1, 2, 3,…, N) are defined, respectively as the jth angular frequency of the decoupled flexural beam and the jth angular frequency of the decoupled shear beam, which are computed by solving the corresponding systems of eigenvalues and eigenvectors for each decoupled beam.

The assumption of classical damping is not appropriate if the system to be analyzed consists of two of more parts with significantly different level of damping, which is the case; therefore, in this paper, the damping matrix for the complete system is constructed by directly assembling the damping matrices for the subsystems through the substructure approach. Accordingly, the damping matrix of matrix equation (18) is assembled as

$$[C_{\mathrm{CTB}}]=\begin{bmatrix}\left[C^F_\Psi\right]+\left[C^F_{\mathrm{d}}\right] & [0]_{(N+2)\times(N+2)}\\ [0]_{(N+2)\times(N+2)} & \left[C^S_\Psi\right]+\left[C^S_{\mathrm{d}}\right]\end{bmatrix} \tag{37}$$

where

$$\left[C^\lambda_\Psi\right]=\begin{bmatrix}\left[C^\lambda_s\right] & [0]_{2\times N}\\ [0]_{N\times2} & \left[C^\lambda_\Delta\right]_{N\times N}\end{bmatrix} \tag{38}$$

$$\left[C^F_{\mathrm{d}}\right]=\left[C^S_{\mathrm{d}}\right]=\begin{bmatrix}[0]_{2\times2} & [0]_{2\times N}\\ [0]_{N\times2} & \frac{1}{2}[C_{\mathrm{d}}]_{N\times N}\end{bmatrix} \tag{39}$$

the superscript $\lambda=F=S$; $[C^F_s]$ and $[C^S_s]$ are the soil's damping matrices defined in Eq. (17); and $[C_{\mathrm{d}}]_{N\times N}$ is the damping matrix of the added linear FVDs, which was defined in Eq. (4).

Based on equation (39), the linear forces exerted by the N FVDs are

split in one half to the flexural cantilever beam and the other half to the shear cantilever beam. This assumption was motivated by mathematical simplicity and is justified and validated in the appendix of this paper by comparing the lateral response between the proposed flexible-base CTB model with FVDs on hard rock and the classic shear-type MDOF system with fixed base and FVDs.

Non-classically damped systems are associated with complex-valued natural modes of vibration, therefore, the concept of modal participating mass ratio, widely used in classical modal analysis, is no longer applicable. Based on the subsystem approach, De Domenico et al. [47] proposed an improved response-spectrum analysis procedure for base-isolated buildings considering the dynamic interaction between the base-isolation-system and the superstructure. On the other hand, De Domenico and Ricciardi [48] introduced two novel measures related to a generalized modal mass ratio and to a modal dissipation ratio of each mode in the complex modal analysis framework for structures equipped with FVDs and base-isolated buildings. In this paper, it is assumed that in the linear range, the system has classic modes, that is, undamped mode shapes, which are necessary for the computation of the damping coefficients of the FVDs. Accordingly, the ith angular frequency w_i and the ith mode shape $\{\varphi_i\}$ of the flexible-base CTB model are obtained by solving the corresponding system of eigenvalues and eigenvectors, where $i = 1,2,3,\ldots, (2N + 4)$. The ith effective modal mass of the flexible-base CTB model is given by

$$m_{eff,i} = \frac{(\{\varphi_i\}^T [M_{CTB}]\{1\}_{(2N+4)\times 1})^2}{\{\varphi_i\}^T [M_{CTB}]\{\varphi_i\}} \tag{40}$$

In this paper, Eq. (18) is solved in time domain by the state space approach [15] due to the non-classically damping of the flexible-base CTB model with FVDs.

3. Numerical examples

The main advantage of the flexible-base CTB model with FVDs is the possibility of considering intermediate modes of lateral deformation. In this section, the proposed CTB model (see Fig. 2) is used to evaluate the dynamic behavior of two tall buildings with different types of lateral deformation.

3.1. 37-story building

A 37-story building located in Mexico City (see Fig. 3a) was considered for the application of the proposed model. Breadth, depth and height of the building are 44 m, 22 m and 144.24 m, respectively. Each story is assumed to have a height of 3.8984 m. The mass per unit length of the building is 235664 kg/m. The building have composite steel deck floors with 4-cm concrete slabs (see Fig. 3b).

Table 1
Mechanical properties of the 37-story building.

Material	Structural element	ρ [kg/m^3]	E [GPa]	ν
Concrete	Floor system	2400	21.57	0.2
	Columns	2400	30.4	0.2
Steel	Beams, columns and braces	7849	200	0.3
Masonry	Shear walls	1300	0.5148	0.3

Table 2
Steel I-beams of the 37-story building.

Steel I-beam	Height [mm]	Mass per unit length [kg/m]
I-1	457	59.8
I-2	838	175.7
I-3	762	147.4
I-4	305	28.2
I-5	406	46.2

Table 3
Steel-concrete composite columns of the 37-story building.

Column	Stories	Dimensions [m x m]
C-1	1 - 9	1.40 x 1.10
C-2	10 - 16	1.40 x 1.00
C-3	17 - 32	1.20 x 1.00
C-4	33 - 37	0.80 x 0.80

The lateral resisting system of the building in x direction consists of moment-resisting frames. On the other hand, the lateral resisting system of the building in y direction consists of a combination of 12-cm masonry shear walls and braced frames. The mechanical properties of the building materials are shown in Table 1.

According to Fig. 3b, the primary steel I-beams (I-2 and I-3) divide the xz plane and yz plane in 37-storey 4-bay frames and 37-storey 2-bay frames, respectively. The dimensions of primary steel I-beams (I-2 and I-3) and secondary steel I-beams (I-1, I-4 and I-5) are shown in Table 2.

Three of the five frames in yz plane are reinforced by 12-cm masonry shear walls and cross steel braces consisting of 356 mm $\times$ 122.1 kg/m steel I-sections: central frame and both external frames. Each story have 15 steel-concrete composite columns (see Fig. 3b) consisting of 356 mm $\times$ 122.1 kg/m steel I-sections encased in rectangular concrete sections that vary along the height (see Table 3).

In order to determine the best values for α in both translational directions, a 3D finite element model (FEM) of the fixed-base 37-story building was developed in a commercial software (see Fig. 4a). The first lateral modes of vibration of the fixed-base 3D FEM are shown in Fig. 4(b) and 4(c).

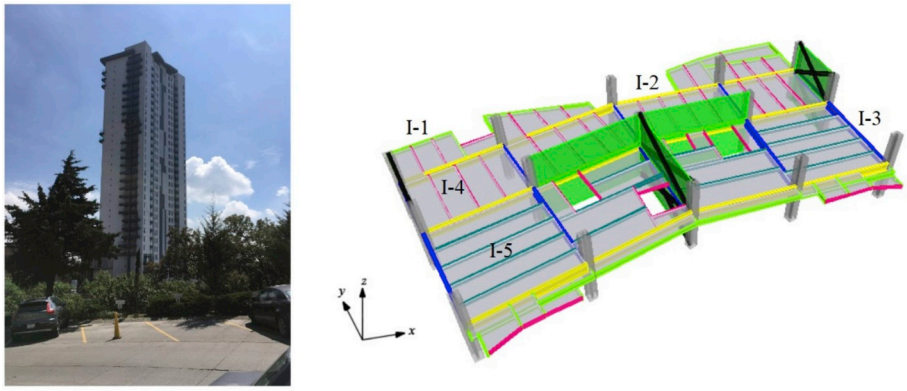

(a) General view (b) Floor system

Fig. 3. 37-story building located in Mexico City.

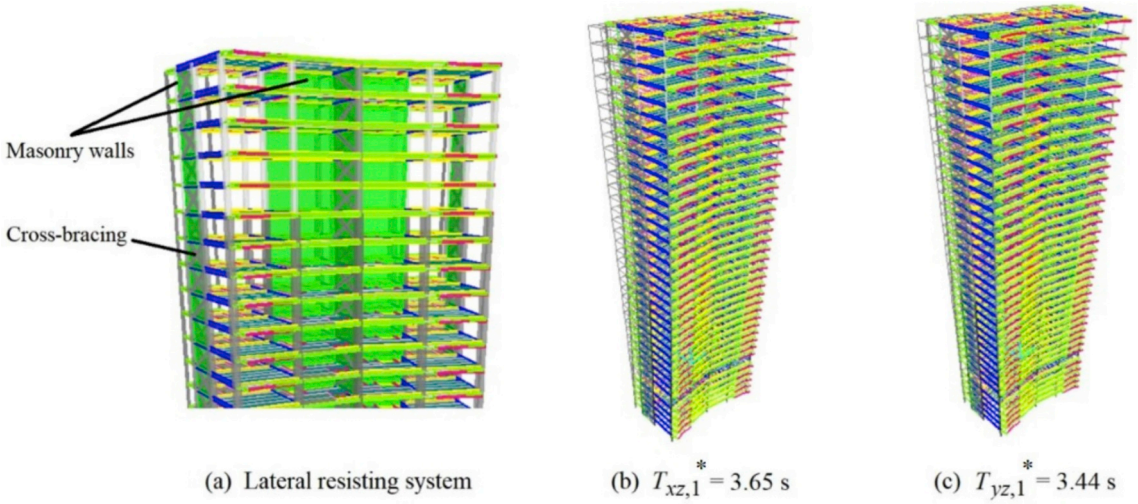

Fig. 4. First lateral modes of vibration of the fixed-base 3D FEM: 37-story building.

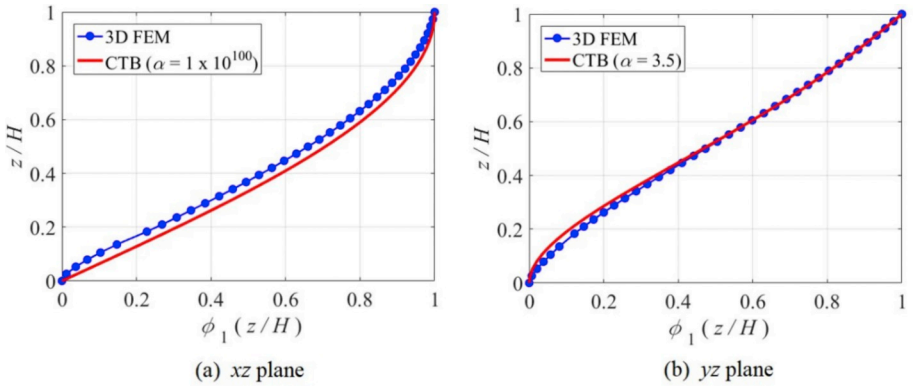

Fig. 5. First modes shapes of the fixed-base 37-story building: 3D FEM vs CTB continuous model.

Table 4
Periods and effective modal masses of the fixed-base 37-story building: CTB model vs 3D FEM.

Mode	Period [s]				Effective modal mass [%]			
	xz plane		yz plane		xz plane		yz plane	
	CTB	3D FEM	CTB	3D FEM	CTB	3D FEM	CTB	3D FEM
1	3.65	3.65	3.44	3.44	80.89	77.26	67.94	66.01
2	1.22	1.25	0.89	0.98	8.84	8.86	13.17	10.62
3	0.73	0.75	0.38	0.48	3.08	2.76	5.71	3.57

According to the 3D FEM of the fixed-base 37-story building (see Fig. 4), the first periods in xz plane and yz plane are 3.65 s and 3.44 s, respectively. On the other hand, the first torsional period is equal to 3.11 s due to asymmetrical plan of the 37-story building, however, the torsion modes are omitted in this paper because the CTB model is only valid for lateral modes of vibration. For buildings with special features, it is highly recommended to perform a more refined analysis.

Fig. 5 compares the computed first lateral mode shapes between the fixed-base 3D FEM and the fixed-base CTB continuous model [2]. According to Fig. 5, $\alpha \to \infty$ (pure shear behavior) for xz plane, where it is assumed that $\alpha = 1 \times 10^{100}$ and $\gamma_1 \approx \pi/2$. On the other hand, a value of $\alpha = 3.5$ fits very well for yz plane, where $\gamma_1 = 1.9235$.

In this numerical example, it was assumed that $(EI)^S = 1 \times 10^{100}$ N m^2 in Eqs. (32) and (34). In addition, it was assumed that all axially rigid members (see Fig. 2) have a spring stiffness $k_j^a = 1 \times 10^{15}$ N/m ($j = 1, 2, 3, \ldots, 37$), guaranteeing the coupling between flexural cantilever beam and shear cantilever beam. A comparison between the CTB continuous model [2] and the 3D FEM is shown in Table 4 for the periods and effective modal masses of the fixed-base 37-story building, which proves that the assumed values of α also adequately represent the higher modes of vibration.

A rigid circular foundation on the ground surface was adopted to explore SSI. For this particular example, it is assumed that the structural plan of the 37-story building has a rectangular shape of 44 m × 22 m;

Table 5
Parameters of the soils and the foundation of the 37-story building.

Soil type	ν_s	ρ_s[kg/m^3]	V_s[m/s]	G_s[GPa]	k_t[GN/m]	k_θ[TN m]	c_t[GN s/m]	c_θ[GN s m]
Hard rock	0.25	2700	2722	20	1600	384	5.95	372
Dense soil	0.33	2400	500	0.6	50.4	12.9	1.02	68
Stiff soil	0.48	1900	300	0.171	15.8	4.74	0.531	41.6
Soft soil	0.49	1800	100	0.018	1.67	0.509	0.169	13.4

Table 6
Periods and effective modal masses of the 37-story building: flexible-base CTB discrete model.

Mode	Soil type	Period [s]		Effective modal mass [%]	
		xz plane($\alpha = 1 \times 10^{100}$)	*yz* plane($\alpha = 3.5$)	*xz* plane($\alpha = 1 \times 10^{100}$)	*yz* plane($\alpha = 3.5$)
1	Hard rock	3.65	3.43	80.97	67.99
	Dense soil	3.75	3.54	80.74	68.50
	Stiff soil	3.92	3.71	80.42	69.31
	Soft soil	5.67	5.53	78.42	73.41
2	Hard rock	1.22	0.90	8.93	13.24
	Dense soil	1.22	0.90	9.25	13.26
	Stiff soil	1.23	0.91	9.76	13.37
	Soft soil	1.30	0.97	13.50	15.48
3	Hard rock	0.73	0.38	3.16	5.71
	Dense soil	0.74	0.39	3.12	5.89
	Stiff soil	0.74	0.40	3.07	6.25
	Soft soil	0.76	0.48	2.79	7.35
4	Hard rock	0.53	0.21	1.57	3.11
	Dense soil	0.53	0.21	1.59	3.40
	Stiff soil	0.53	0.22	1.63	4.01
	Soft soil	0.55	0.29	1.80	2.22

therefore, the radius for an equivalent circular foundation is $r_0 = \sqrt{A_0/\pi}$, where A_0 is the area of the foundation. Accordingly, m_0, $I_{m,0}$ and r_0 are 1.84 x 10^6 kg, 1.41 x 10^8 kg m^2 and 17.55 m, respectively. Four types of soil [49] were chosen to carry out the dynamic analysis of the 37-story building: (1) hard rock, (2) dense soil, (3) stiff soil and (4) soft soil. Table 5 summarizes parameters of the soils and the foundation of the 37-story building.

For both translational directions and the parameters of Table 5, Table 6 shows the periods of vibration and effective modal masses of the first four modes of vibration computed by the flexible-base CTB model.

The effect of soil flexibility on different lateral resisting systems can be studied thanks to the similar values of $T_{xz,1}$ and $T_{yz,1}$ for the four soil types (see Table 6), in spite of the remarkable difference between the lateral resisting systems of the 37-story building: $\alpha = 1 \times 10^{100}$and $\alpha = 3.5$ for *xz* plane and *yz* plane, respectively. Table 6 shows that the first mode of vibration changes significantly as the soil flexibility increases, but the higher modes of vibration are less affected. On the other hand, periods of higher modes increase as the flexural rigidity of the building decreases. For *xz* plane ($\alpha = 1 \times 10^{100}$), the first effective modal mass decreases as the soil flexibility increases; conversely, for *yz* plane ($\alpha = 3.5$), the first effective modal mass increases as the soil flexibility increases. The effective modal masses of higher modes are also affected as the soil flexibility and lateral resisting system change.

For a particular translational direction, the three distribution methods for linear FVDs [29] (UD, SSPD and SSSED) depend on the first period of vibration and its associated mode shape (Eqs. (7)–(9)). For this reason, only the first mode shape of the 37-story building is shown in Fig. 6 for the four soil types and both translational directions.

For a pre-design stage, it is assumed that the high-rise building has 37 K-brace chevron linear FVDs (one per each story), in other words, this means that all magnifications factors f_j(j=1,2,3,…,37) are equal to 1. Assuming that $\xi_d = 0.15$, the damping coefficients of the FVDs were computed for the 37-story building through the three distribution methods [29] (see Figs. 7–10).

Figs. 7–10 show that for a UD, the damping coefficients of the FVDs increase as the flexural rigidity of the building decreases; which shows that the typical MDOF shear building model overestimates the damping coefficients of uniform FVDs in medium-rise to high-rise buildings, where the flexural deformation is as significant as the shear deformation. For SSPD and SSSED methods, the damping coefficients of the FVDs vary along the height of the building depending on the lateral resisting system. For the three distribution methods and the same lateral deformation, the damping coefficients of the FVDs decrease as the soil flexibility increases.

3.1.1. *Earthquake-induced vibrations*

As is well known, earthquakes having different origins affect Mexico City. There exist four groups: (1) local earthquakes; (2) continental-plate earthquakes; (3) normal-faulting earthquakes and (4) subduction earthquakes. It has been observed that the normal-faulting [50–53] and subduction earthquakes [54,55] are the most dangerous events for Mexico City. For building code purposes, the subsoil of Mexico City has been divided in three zones: (1) the hill zone, characterized by a surface layer of lava flows or volcanic tuff; (2) the transition zone, composed of alluvial sandy and silty layers with occasional intervals of clay layers; and (3) the lake bed zone, consisting of 10 to 80 m deposit of highly compressible and high water content clay underlain by resistant sands. The relative amplification of ground motions in the lake bed zone with respect to those in the hill zone of the city is a well-known phenomenon, the motion in the lake bed zone is 8 to 50 times in the frequency domain with respect to a hill zone site. This was dramatically demonstrated during the September 1985 earthquakes that caused significant damage

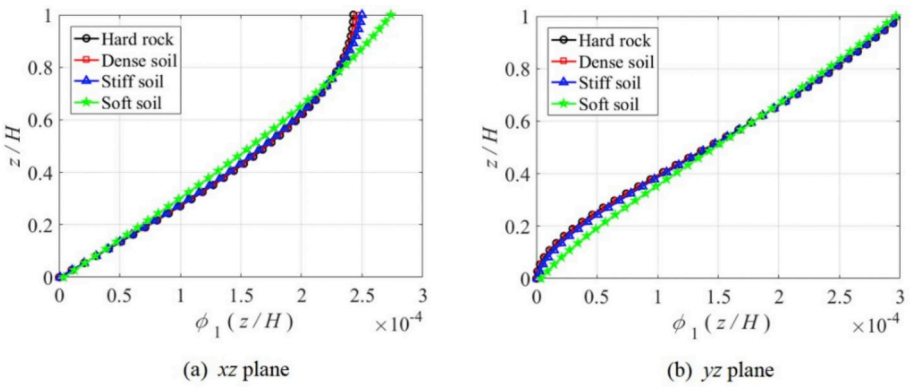

Fig. 6. First mass normalized mode shapes of the 37-story building: flexible-base CTB discrete model.

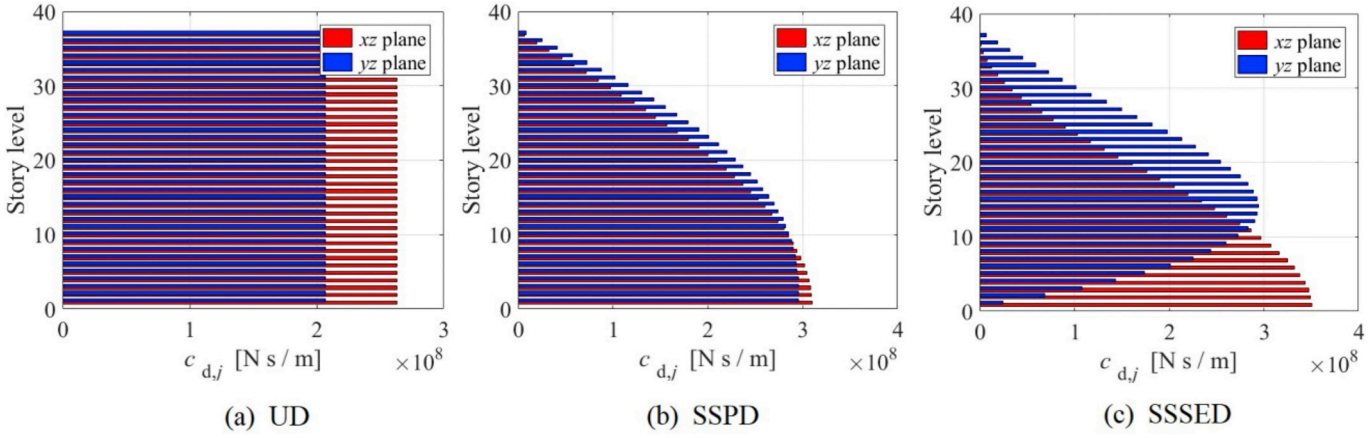

Fig. 7. Damper coefficient distribution for different design methods: 37-story building on hard rock.

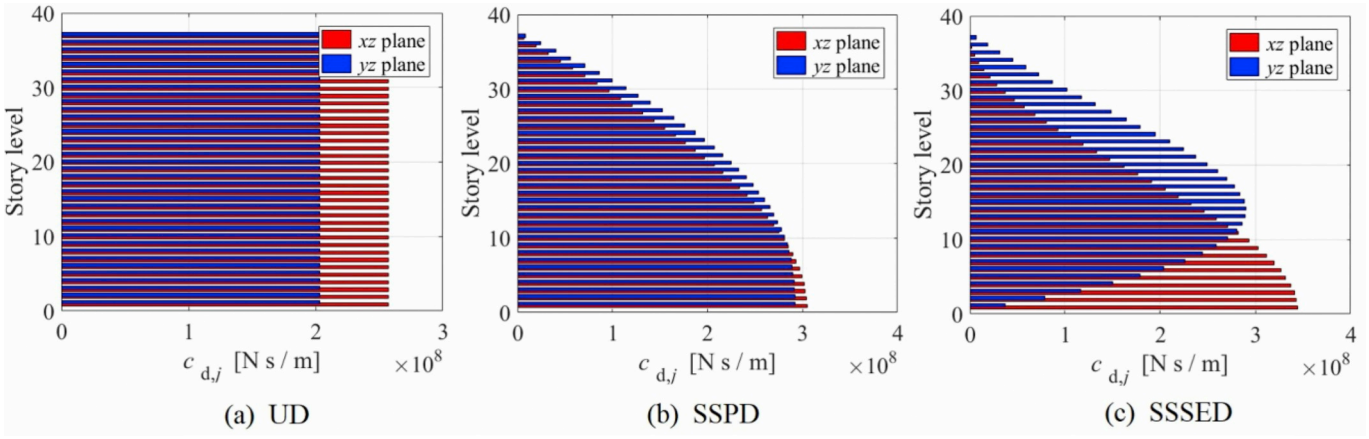

Fig. 8. Damper coefficient distribution for different design methods: 37-story building on dense soil.

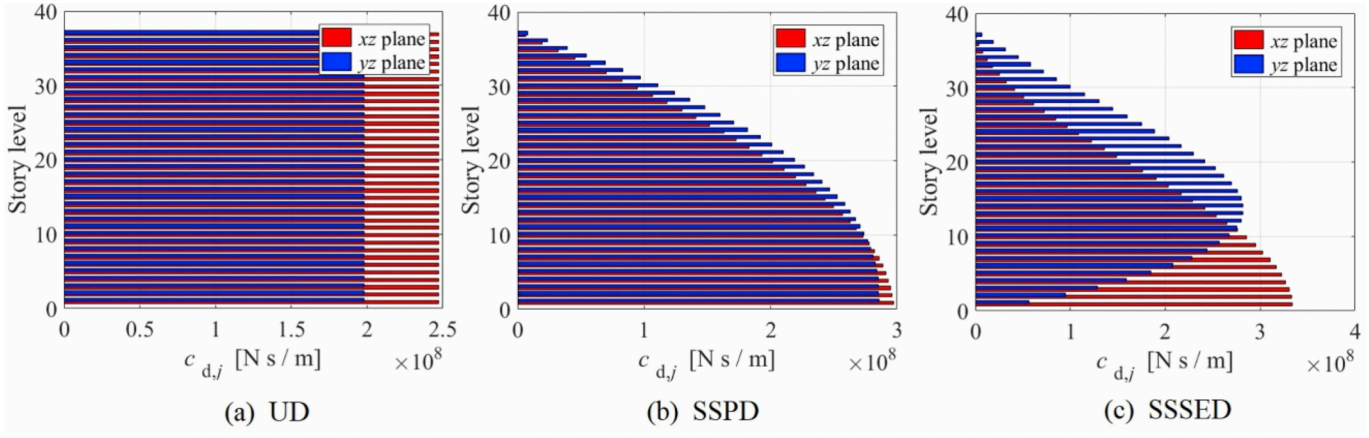

Fig. 9. Damper coefficient distribution for different design methods: 37-story building on stiff soil.

and the loss of thousands of lives in this city, the heavy damage to mid-rise (7-15-storey) buildings was quite impressive, in spite of the light damage to low-rise and high-rise buildings, and other structures. The predominant periods of ground surface in disastrous areas were in the range of 1.5 a 2.5 s [56]. Site effects in Mexico City are increasing as a consequence of ground subsidence produced by groundwater withdrawal [57,58].

The application of several recorded ground motions from different seismic sources that affect buildings in Mexico [50,54,55] will be carried out in future works, since the objective of this paper is only the proposal of the flexible-base CTB model with FVDs (see Fig. 2). For this reason, it was considered that the 37-story building was subjected to the horizontal ground accelerations recorded at station Central--de-Abastos-Frigorífico (CDAF) during the Mexico City earthquake of September 19, 1985. Station CDAF is located in Mexico City on the lake bed zone (clay soil). The horizontal ground accelerations and elastic input energy spectrum with a modal damping ratio of 5% are shown in Fig. 11 for the Mexico City earthquake of September 19, 1985 at station

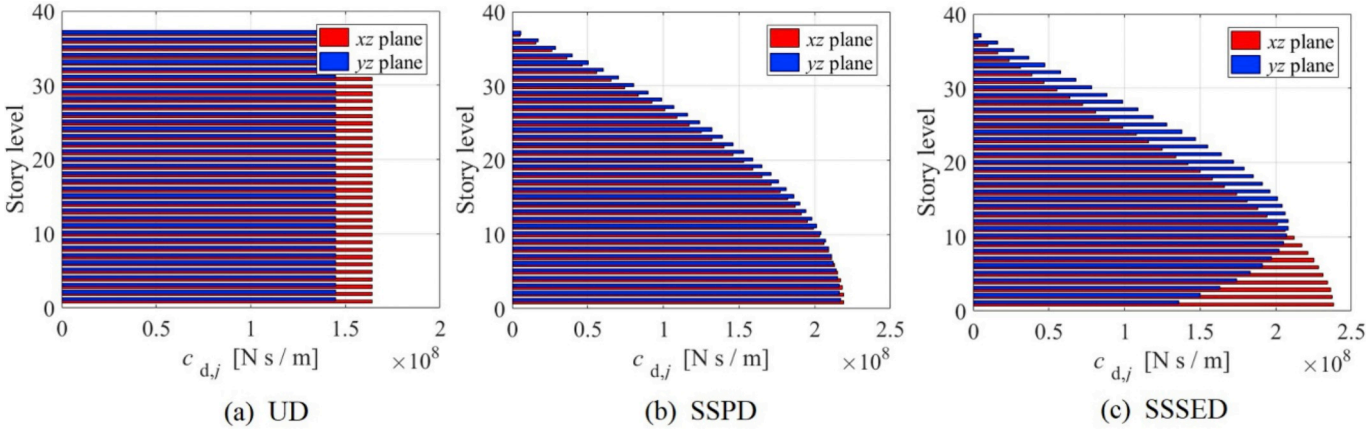

Fig. 10. Damper coefficient distribution for different design methods: 37-story building on soft soil.

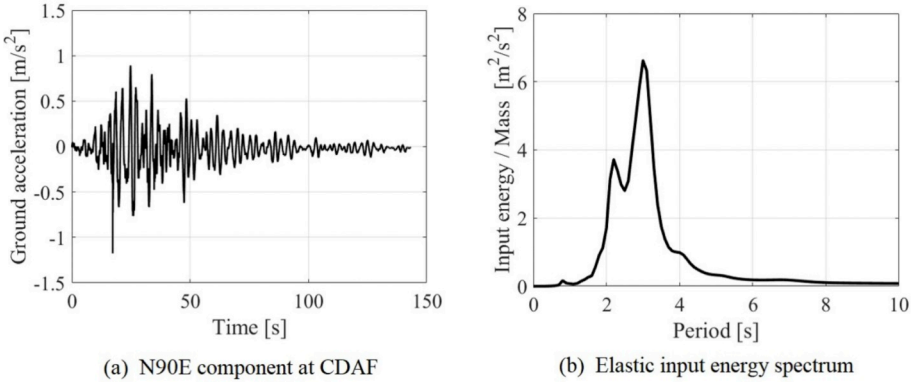

Fig. 11. Mexico City earthquake of September 19, 1985: station CDAF (lake bed zone).

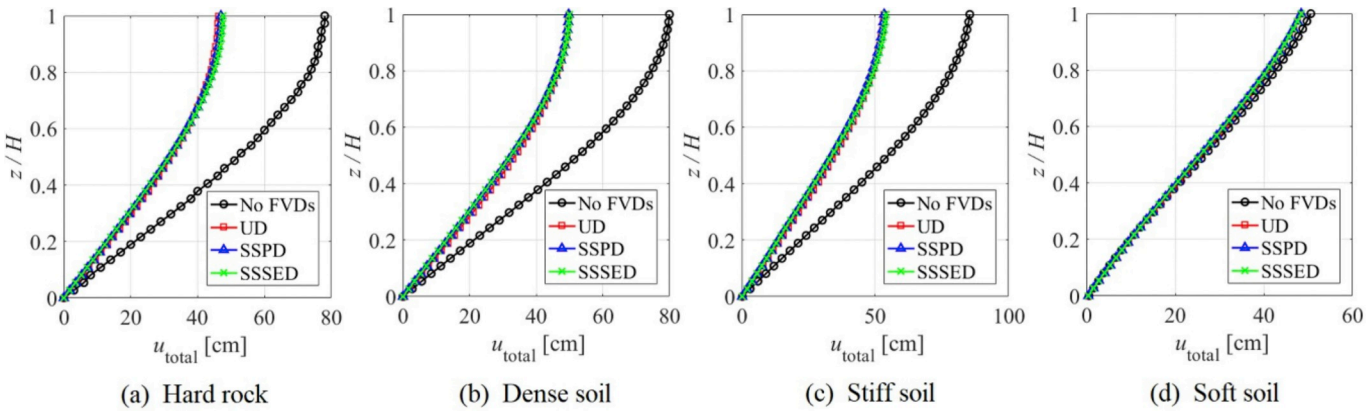

Fig. 12. Total seismic peak displacement profiles: *xz* plane of the 37-story building at station CDAF.

CDAF; where the peak input energy per unit mass (6.67 m^2/s^2) is related to a period of vibration of 3.05 s.

A time-history elastic analysis was carried out for the 37-story building when it is subjected to the horizontal ground accelerations shown in Fig. 11a. The soil-foundation parameters and the FVDs parameters were taken from Table 5 and Figs. 7–10, respectively. The total peak displacement profiles are shown in Figs. 12 and 13, considering a structural damping of 5% for the first two modes of vibration of the fixed-base building.

Figs. 12 and 13 show that total peak displacements increase as the flexural rigidity of the building increases; which shows that the typical MDOF shear building model underestimates the seismic response in medium-rise to high-rise buildings, where the flexural deformation is as significant as the shear deformation. For no FVDs case, the smallest displacements occur on a soft soil because the periods of the first mode in both translational directions elongate too enough to avoid the resonance of the 37-story building (see Fig. 11 b). For the same soil type and the same value of, the three distribution methods achieve practically the same total peak displacements; on the contrary, the seismic response control varies significantly as the soil type and lateral resisting system change. For the three distribution methods and the same value of α, there is a significant decrease in controlling earthquake-induced vibrations as the soil flexibility increases.

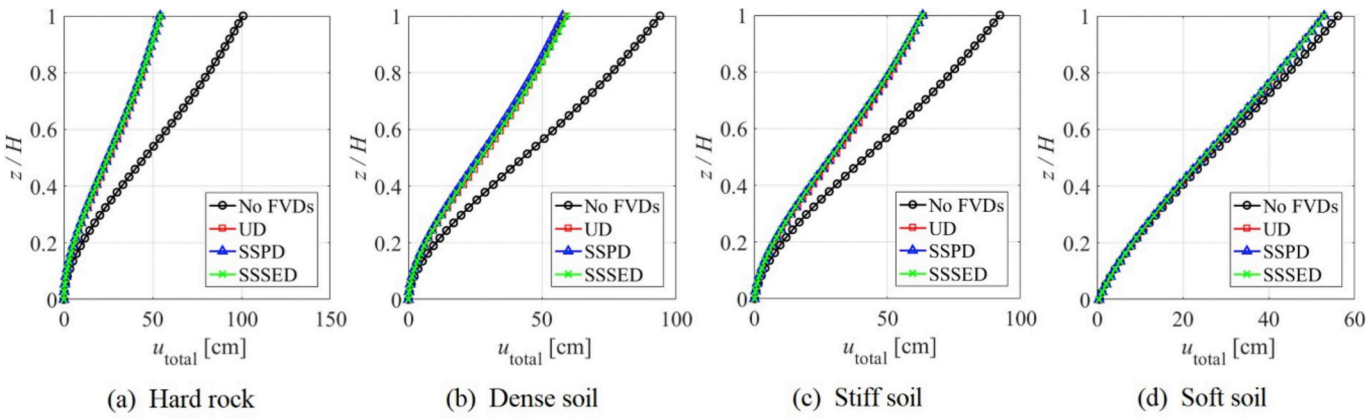

Fig. 13. Total seismic peak displacement profiles: *yz* plane of the 37-story building at station CDAF.

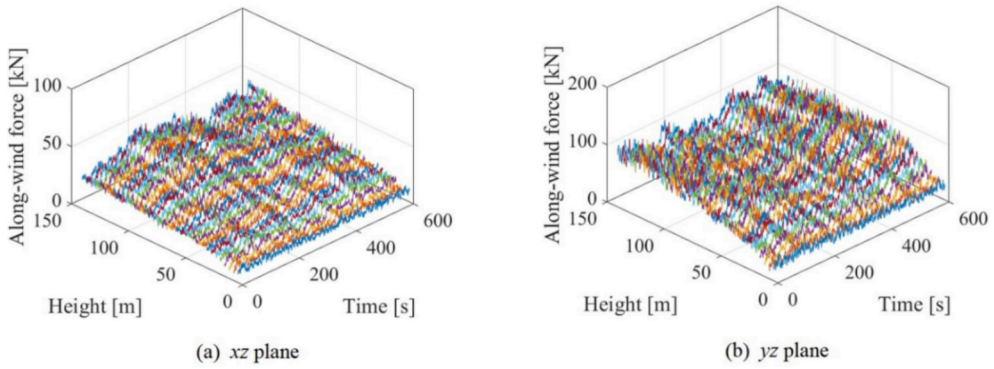

Fig. 14. Along-wind forces for the 37-story building.

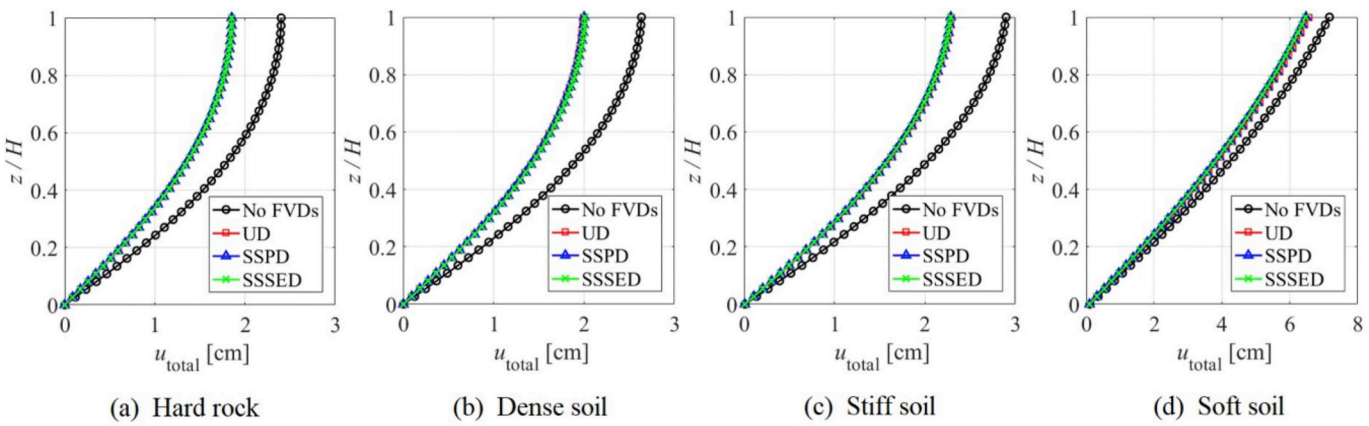

Fig. 15. Total along-wind peak displacement profiles: *xz* plane of the 37-story building.

3.1.2. Wind-induced vibrations

The 37-story building is located in a suburban area with a roughness length of 0.3 m. Assuming an annual probability of 0.02, the mean wind velocity at 10 m height is equal to 15.02 m/s [59]. Synthetic along-wind time series were simulated assuming a rectangular tall building with drag coefficients of 1.1 and 1.45 for *xz* plane and *yz* plane, respectively [60]. The simulated along-wind time series for the 37-story building are shown in Fig. 14.

A time-history elastic analysis was carried out for the 37-story building when it is subjected to the along-wind forces shown in Fig. 14. The soil-foundation parameters and the FVDs parameters were taken from Table 5 and Figs. 7–10, respectively. For a total dynamic response, the peak displacements and RMS accelerations are shown in Figs. 15 to 18. RMS accelerations are usually used to check the serviceability limit state, which is why these are shown instead of the peak accelerations. A structural damping of 1% was considered for the first two modes of vibration of the fixed-base building.

Figs. 15 to 18 show that the total dynamic response increases as the flexural rigidity of the building increases; in a similar way, the total dynamic response increases as the soil flexibility increases. Therefore, the along-wind response in medium to high-rise buildings will be underestimated if a fixed-base MDOF shear building is used instead the flexible-base CTB model. For the same soil type and the same value of α, the three distribution methods achieve practically the same total

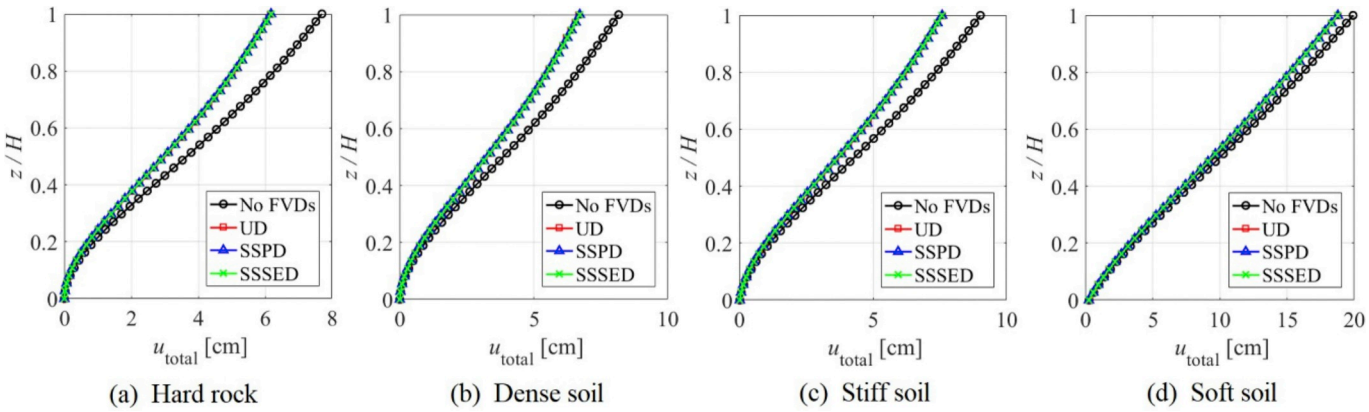

Fig. 16. Total along-wind peak displacement profiles: *yz* plane of the 37-story building.

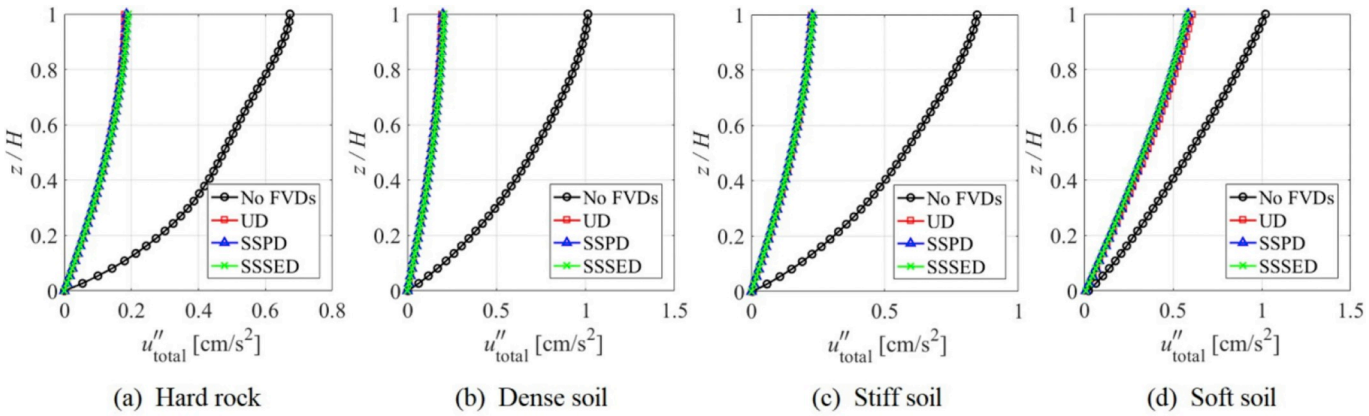

Fig. 17. Total along-wind RMS acceleration profiles: *xz* plane of the 37-story building.

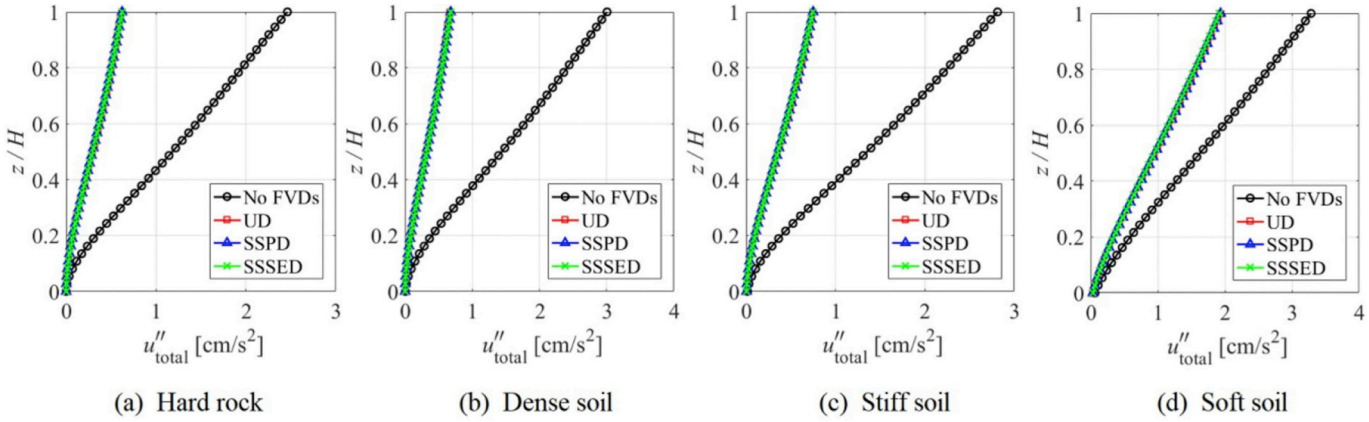

Fig. 18. Total along-wind RMS acceleration profiles: *yz* plane of the 37-story building.

dynamic response; on the contrary, the along-wind response control varies significantly as the soil type and lateral resisting system change. For the three distribution methods and the same value of α, there is a significant decrease in controlling wind-induced vibrations as the soil flexibility increases. Generally speaking, FVDs are more effective for controlling RMS accelerations compared to peak displacements induced by along-wind loads.

3.2. 25-story building

A 25-story building located in Mexico City (see Fig. 19a) was considered for the application of the proposed model. Breadth, depth and height of the building are 25 m, 25 m and 93.65 m, respectively. Each story is assumed to have a height of 3.746 m. The mass per unit length of the building is 112500 kg/m. The lateral resisting system consists of a combination of braced frames and shear walls (see Fig. 19b). The mechanical properties and dimensions of the structural elements of the 25-story building are described in detail by Huergo and Hernández [7].

In this numerical example, only the *yz* plane of the 25-story building is analyzed (see Fig. 19b). For the *yz* plane, T_1^*, α and γ_1 are 2.09 s, 6.5 and 1.8143, respectively [7]. It was assumed that $(E\,I)^S = 1 \times 10^{100}$ N m^2 and $k_j^a = 1 \times 10^{15}$ N/m, where $j = 1, 2, 3, \ldots, 25$. A rigid circular foundation on the ground surface was adopted to explore SSI.

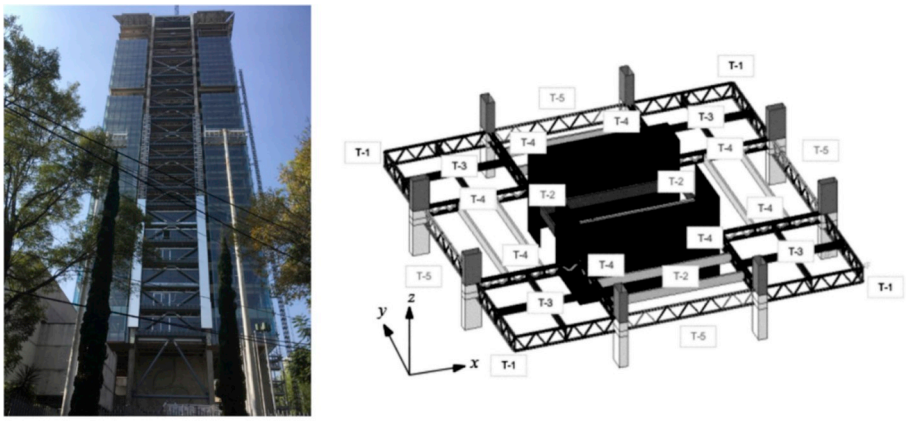

(a) General view; (b) Floor system.

Fig. 19. 25-story building in Mexico City.

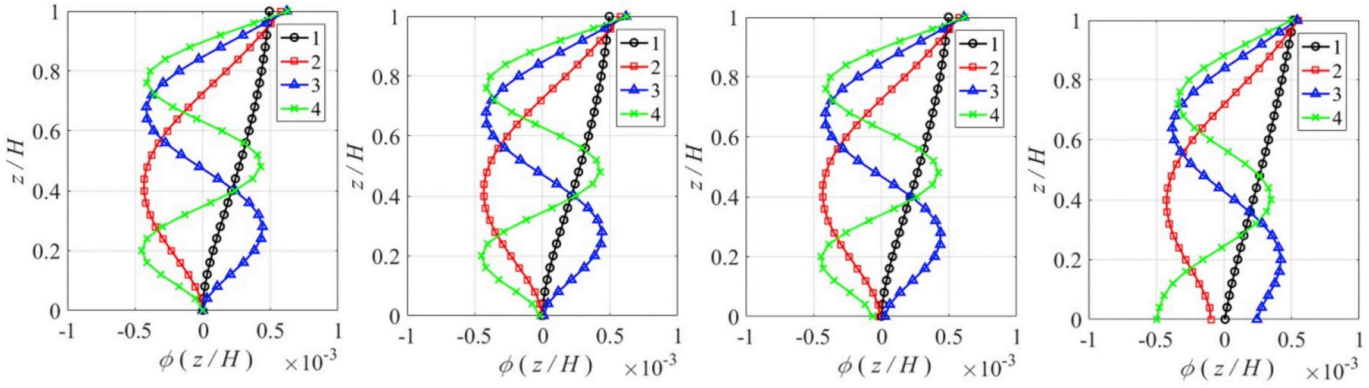

(a) Hard rock (b) Dense soil (c) Stiff soil (d) Soft soil

Fig. 20. Mass normalized mode shapes of the flexible-base 25-story building: *yz* plane ($\alpha = 6.5$).

Table 7
Periods and effective modal masses of the fixed-base 25-story building: *yz* plane [7].

Mode	Period [s]		Effective modal mass [%]	
	Fixed-base CTB($\alpha = 6.5$)	Fixed-base 3D FEM	Fixed-base CTB($\alpha = 6.5$)	Fixed-base 3D FEM
1	2.09	2.09	72.30	74
2	0.62	0.62	10.57	17
3	0.31	0.30	4.77	4.22

m_0, $I_{m,0}$ and r_0 are 8.43 x 10^5 kg, 3.29 x 10^7 kg m^2 and 12.5 m, respectively [8]. A comparison between the CTB continuous model [2] and the 3D FEM [7] is shown in Table 7 for the periods and effective modal masses of the fixed-base 25-story building, where a value of $\alpha = 6.5$ develops an excellent match for the *yz* plane of the 25-story building because the evident nature of parallel coupling of the lateral resisting system.

Four types of soil [49] were chosen to carry out the dynamic analysis of the 25-story building: (1) hard rock, (2) dense soil, (3) stiff soil and (4) soft soil. Table 8 summarizes parameters of the soils and the foundation of the 25-story building.

For the soil parameters of Table 8, Table 9 shows the periods of vibration and effective modal masses of the first four modes of vibration computed by the flexible-base CTB model.

For a pre-design stage, it is assumed that the high-rise building has 25 K-brace chevron linear FVDs (one per each story), in other words, this means that all magnifications factors $f_j (j=1,2,3,\ldots,25)$ are equal to 1. Assuming that $\xi_d = 0.15$, the damping coefficients of the FVDs were computed for the 25-story building through the three distribution methods [29] (see Fig. 21).

For the three distribution methods (UD, SSPD and SSSED), Fig. 21 shows that the damping coefficients of FVDs of the 25-story building decrease as the soil flexibility increases.

3.2.1. *Earthquake-induced vibrations*

In this numerical example, only earthquake-induced vibrations are considered. The application of several recorded ground motions from

Table 8
Parameters of the soils and the foundation: *yz* plane of the 25-story building.

Soil type	ν_s	ρ_s[kg/m^3]	V_s[m/s]	G_s[GPa]	k_t[GN/m]	k_θ[TN m]	c_t[GN s/m]	c_θ[GN s m]
Hard rock	0.25	2700	2722	20	1140	139	3.02	95.7
Dense soil	0.33	2400	500	0.6	35.9	4.66	0.516	17.5
Stiff soil	0.48	1900	300	0.171	11.3	1.71	0.270	10.7
Soft soil	0.49	1800	100	0.018	1.19	0.184	0.0857	3.45

Table 9
Periods and effective modal masses of the flexible-base 25-story building: *yz* plane ($\alpha = 6.5$). The mode shapes related to Table 9 are shown in Fig. 20.

Mode	Period [s]				Effective modal mass [%]			
	Hard rock	Dense soil	Stiff soil	Soft soil	Hard rock	Dense soil	Stiff soil	Soft soil
1	2.10	2.16	2.27	3.36	72.28	72.54	72.98	75.16
2	0.62	0.62	0.62	0.66	10.55	10.66	10.88	13.68
3	0.31	0.31	0.31	0.35	4.76	4.82	4.96	5.89
4	0.18	0.18	0.18	0.23	2.76	2.89	3.20	2.71

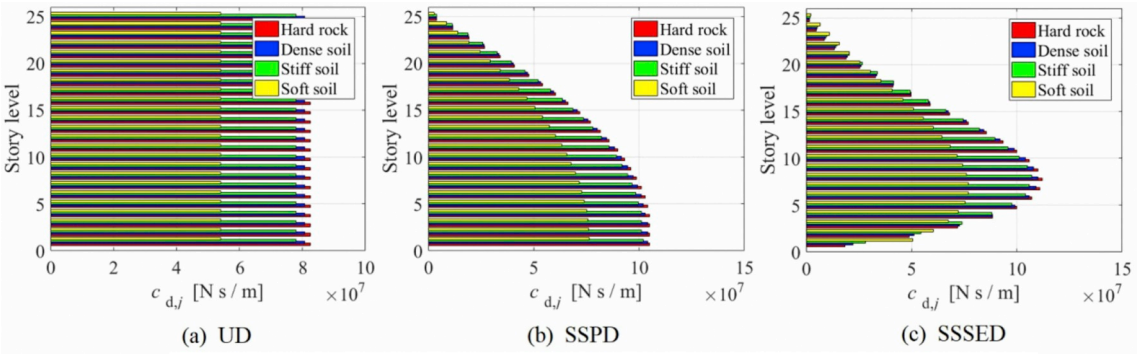

Fig. 21. Damper coefficient distribution for different design methods: *yz* plane of the 25-story building.

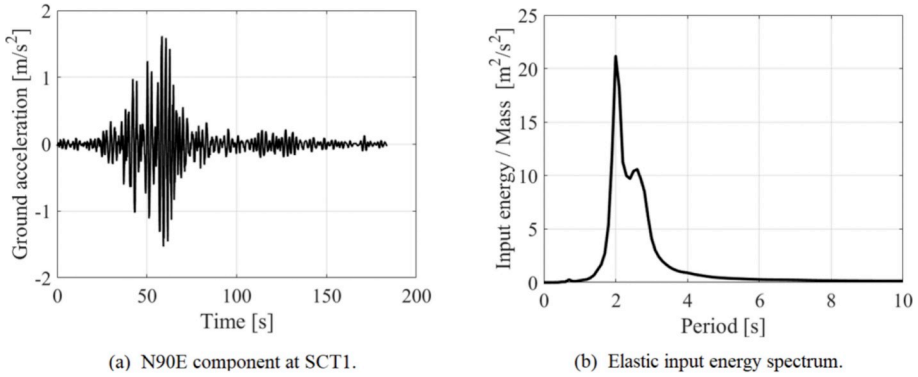

Fig. 22. Mexico City earthquake of September 19, 1985: station SCT1 (lake bed zone).

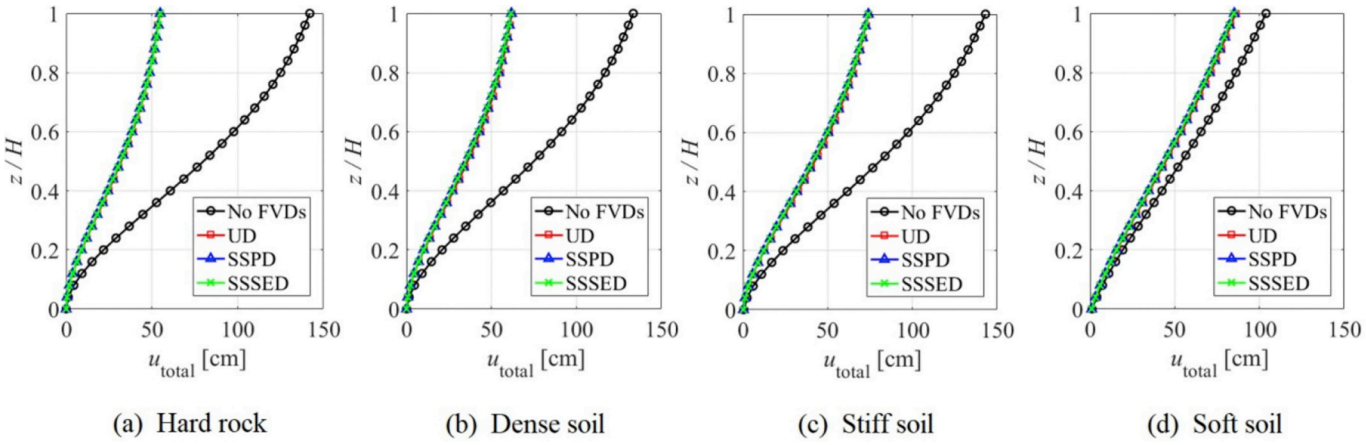

Fig. 23. Total seismic peak displacement profiles: *yz* plane of the 25-story building at station SCT1.

different seismic sources that affect buildings in Mexico [50,54,55] will be carried out in future works. It was assumed that the 25-story building was subjected to the horizontal ground accelerations recorded at station SCT1 during the Mexico City earthquake of September 19, 1985. Station SCT1 is located on the lake bed zone (clay soil). The horizontal ground accelerations and elastic input energy spectrum with a modal damping ratio of 5% are shown in Fig. 22 for the Mexico City earthquake of September 19, 1985 at station SCT1; where the peak input energy per unit mass (21.83 m^2/s^2) is related to a period of vibration of 2.05 s.

A time-history elastic analysis was carried out for the 25-story

building when it is subjected to the horizontal ground accelerations shown in Fig. 22a. The soil-foundation parameters and the FVDs parameters were taken from Table 8 and Fig. 21, respectively. The total peak displacements are shown in Fig. 23, considering a structural damping of 5% for the first two modes of vibration of the fixed-base building.

Fig. 23 shows that the smallest displacements occur on a soft soil because the first period in *yz* plane elongates too enough to avoid the resonance of the 25-story building (see Fig. 22 b). For the same soil type, the three distribution methods achieve practically the same total peak displacements for the *yz* plane of the 25-story building. On the other hand, the three distribution methods achieve a significant decrease in controlling earthquake-induced vibrations as the soil flexibility increases.

4. Conclusions

Low-rise buildings laterally deform like pure shear beams; however, in medium-rise to high-rise buildings, the flexural deformation is as significant as the shear deformation due to the evolution of lateral resisting systems. The most recent distribution methods for FVDs strongly depend on the fundamental mode of vibration, which changes depending on the soil flexibility and the type of lateral resisting system of the building. However, scientific literature shows that MDOF shear building models are commonly used to represent low-, medium- and high-rise buildings with FVDs, either with or without SSI.

The CTB model seems the better model for estimating the frequencies and mode shapes in buildings with different lateral resisting systems, particularly in shear wall-frame buildings and tube-and-core constructions with the parallel nature of the two-beam model in which transverse displacements due to bending and to shear are identical. In this paper, a flexible-base CTB model with FVDs is presented to compute the dynamic response in time domain of two high-rise buildings with different types of lateral deformation and considering different soil types and three different distribution methods for linear FVDs (UD, SSPD and SSSED). The proposed formulation is only valid for planar models, that is, it is not able to consider torsional effects.

Accordingly, the following conclusions were obtained for the dynamic properties of the two high-rise buildings:

(a) The first period of vibration significantly elongates as the soil flexibility increases. Conversely, the periods of higher modes slightly elongate as the soil flexibility increases.
(b) For a pure shear behavior, a cumulative effective modal mass adding up to 90% of the total mass is reached when the first two modes of vibration are considered. On the other hand, the same cumulative effective modal mass is reached when the first four modes of vibration are considered for a lateral deformation close to a pure flexural beam.
(c) For a lateral deformation close to a pure shear beam, the first effective modal mass decreases as the soil flexibility increases. Conversely, for a lateral deformation close to a pure flexural beam, the first effective modal mass increases as the soil flexibility increases.

On the other hand, the following conclusions were obtained for the same value of the supplemental damping ratio, different soil types and three different distribution methods for linear FVDs (UD, SSPD and SSSED):

(d) For a UD, the damping coefficients of the FVDs increase as the flexural rigidity of the building decreases; which shows that the typical MDOF shear building model overestimates the damping coefficients of uniform FVDs in medium-rise to high-rise buildings, where the flexural deformation is as significant as the shear deformation.
(e) For SSPD and SSSED methods, the damping coefficients of the FVDs vary along the height of the building depending on the lateral resisting system. For a lateral deformation close to a pure flexural beam, the damping coefficients of the FVDs are greater in the upper stories; whereas, for a lateral deformation close to a pure shear beam, the damping coefficient of the FVDs are greater in the lower stories.
(f) For the three distribution methods (UD, SSPD and SSSED) and the same lateral deformation, the damping coefficients of the FVDs decrease as the soil flexibility increases.
(g) For the same soil type and the same lateral deformation, the three distribution methods (UD, SSPD and SSSED) achieve practically the same total dynamic response.
(h) For the three distribution methods (UD, SSPD and SSSED) and the same lateral deformation, there is a significant decrease in controlling earthquake-induced vibrations and wind-induced vibrations as the soil flexibility increases.

In future works, nonlinear FVDs will be studied by the proposed model through existing linearization procedures considering several ground motions from different seismic sources and several simulated along-wind time series with different turbulence intensities. In addition, the proposed CTB scheme will be implemented with incorporation of an optimal design strategy for the FVD distribution along the building height. On the other hand, possible extensions of the procedure to spatial 3D frames will also be studied in future works.

Funding information

CONACyT – Becas México.

Acknowledgments

The authors would like to acknowledge CONACyT – Becas México for the financial support to the first author for conducting doctoral studies at Universidad Nacional Autónoma de México under the supervision of the second author. The authors also wish to thank Universidad Nacional Autónoma de México and Universidad Michoacana de San Nicolás de Hidalgo.

APPENDIX

The pre-design stage of buildings with FVDs is usually based on fixed-base MDOF shear building models [9], where m_j(j=1,2,3,…,N), k_j(j=1,2,3,…, N) and c_j(j=1,2,3,…,N) represent, respectively the mass, the lateral stiffness and the damping coefficient of the jth story of the shear building. Establishment and solution of the equations of motion of a fixed-base MDOF shear building with linear FVDs has been widely studied in literature [9].

The 37-story building (see Fig. 4) deforms like a pure shear beam in the *xz* plane ($\alpha \rightarrow \infty$), on the contrary, it has intermediate modes of lateral deformation in the *yz* plane($\alpha = 3.5$). Therefore, the validation of the flexible-base CTB model with FVDs (see Fig. 2) only can be performed for the *xz* plane of the 37-story building if it is assumed a hard rock condition. Accordingly, it is assumed that the fixed-base MDOF shear building model with FVDs [9] can reproduce the same results for the *xz* plane of the 37-story building on hard rock.

The lateral stiffness of the columns of the 37-story building (see Fig. 4) decreases along height (see Table 3); however, Miranda and Reyes [45]

concluded that maximum interstory drift demands in the fixed-base CTB continuous model [2] were not significantly influenced by reductions in stiffness along the height, provided that no abrupt reductions in stiffness occur. Assuming a fixed-base shear building model in the *xz* plane of the 37-story building, m_j(j=1,2,3,..,36), m_{37} andk_j(j=1,2,3,..,37) are 9.1871 x 10^5 kg, 4.5935 x 10^5 kg and 1.5071 x 10^9 N/m, respectively. For the horizontal ground accelerations shown in Fig. 11a, the damping coefficients c_j(j=1,2,3,…,N) are computed assuming a Rayleigh damping [46] and structural damping ratios equal to 5%.

Table A.1 shows the periods of vibration and effective modal masses of the first four modes of vibration computed by both models for the *xz* plane of the 37-story building.

TABLE A.1Periods and effective modal masses of the 37-story building on hard rock: *xz* plane

i	Period [s]		Effective modal mass [%]	
	Fixed-base MDOF shear building	CTB on hard rock($\alpha = 1 \times 10^{100}$)	Fixed-base MDOF shear building	CTB on hard rock($\alpha = 1 \times 10^{100}$)
1	3.65	3.65	81.06	80.97
2	1.22	1.22	9.01	8.93
3	0.73	0.73	3.24	3.16
4	0.52	0.53	1.65	1.57

Tables A.2 shows the elastic seismic response at rooftop level when the 37-story building is subjected to the horizontal ground accelerations shown in Fig. 11a.

TABLE A.2Total seismic peak displacements [cm] at rooftop level for a hard rock condition: *xz* plane

Design methodology	Fixed-base MDOF shear building	CTB on hard rock ($\alpha = 1 \times 10^{100}$)
No FVDs	77.72	77.77
UD for 37 K-brace chevron FVDs ($\xi_d = 15\%$)	45.99	46.13
SSPD for 37 K-brace chevron FVDs ($\xi_d = 15\%$)	46.81	46.96
SSSED for 37 K-brace chevron FVDs ($\xi_d = 15\%$)	47.45	47.56

Tables A.1 and A.2 show that periods, effective modal masses and elastic seismic response are equal for engineering purposes, which validates the flexible-base CTB model with FVDs (see Fig. 2).

References

[1] Rahgozar R, Safari H, Kaviani P. In: Jones N, Brebbia CA, editors. Structures under shock and impact VIII. U.K: WIT Press; 2004. https://doi.org/10.2495/SU040231.
[2] Miranda E, Taghavi S. J Struct Eng 2005;131:203. https://doi.org/10.1061/(ASCE)0733-9445(2005)131:2(203).
[3] Dym CL, Williams HE. J Struct Eng 2007;133:1479. https://doi.org/10.1061/(ASCE)0733-9445(2007)133:10(1479).
[4] Cruz C, Miranda E. Soil Dyn Earthq Eng 2017;100:183. https://doi.org/10.1061/(ASCE)ST.1943-541X.0001628.
[5] Cruz C, Miranda E. J Eng Struct 2017;138:324. https://doi.org/10.1016/j.engstruct.2017.02.001.
[6] Wu D, Zhao B, Lu X. Soil Dyn Earthq Eng 2018;115:365. https://doi.org/10.1016/j.soildyn.2018.07.043.
[7] Huergo IF, Hernández H. Struct Des Tall Special Build 2019. https://doi.org/10.1002/tal.1671.
[8] Huergo IF, Hernández H. Struct Des Tall Special Build 2019. https://doi.org/10.1002/tal.1683.
[9] De Domenico D, Ricciardi G, Takewaki I. Soil Dyn Earthq Eng 2019;118:144. https://doi.org/10.1016/j.soildyn.2018.12.024.
[10] Lin WH, Chopra AK. Earthq Eng Struct Dyn 2002;31:1623. https://doi.org/10.1002/eqe.179.
[11] Di Paola M, Navarra G. Struct Control Health Monit 2009;16:303. https://doi.org/10.1002/stc.254.
[12] De Domenico D, Ricciardi G. Soil Dyn Earthq Eng 2018;113:415. https://doi.org/10.1016/j.soildyn.2018.06.015.
[13] De Domenico D, Ricciardi G. Eng Struct 2019;179:523. https://doi.org/10.1016/j.engstruct.2018.09.076.
[14] Zen X, Peng Y, Chen J. Struct Des Tall Special Build 2017;26. https://doi.org/10.1002/tal.1371.
[15] Hart GC, Wong K. Structural dynamics for structural engineers. first ed. United States of America: John Wiley & Sons, Inc.; 1999.
[16] Xu YL, He Q, Ko JM. Eng Struct 1999;21:135. https://doi.org/10.1016/S0141-0296(97)00154-5.
[17] Patel CC, Jangid RS. Struct Control Health Monit 2014;21:205. https://doi.org/10.1002/stc.1566.
[18] Rama K, Ansu M, Iyer N. Struct Control Health Monit 2013;21:342. https://doi.org/10.1002/stc.1568.
[19] Halperin I, Ribakov Y, Agranovich G. Struct Control Health Monit 2015;23:458. https://doi.org/10.1002/stc.1779.
[20] Apostolakis G, Dargush GF. Earthq Eng Struct Dyn 2010;39:355. https://doi.org/10.1002/eqe.944.
[21] Wong HL, Luco JE. J. Eng Mech ASCE 1991;117:2237. https://doi.org/10.1061/(ASCE)0733-9399(1991)117:10(2237).
[22] Alam S, Baba S. J. Eng Mech ASCE 1993;119:2533. https://doi.org/10.1061/(ASCE)0733-9445(1993)119:9(2533).
[23] Smith HA, Wu WH, Borja RI. Earthq Eng Struct Dyn 1994;23:609. https://doi.org/10.1002/eqe.4290230604.
[24] Smith HA, Wu WH. Earthq Eng Struct Dyn 1997;26:549. https://doi.org/10.1002/(SICI)1096-9845(199705)26:5<549::AID-EQE662>3.0.CO;2-2.
[25] Zhao X, Wang S, Du D, Liu W. Earthq Eng Eng Vib 2017;16:199. https://doi.org/10.1007/s11803-017-0377-x.
[26] Takewaki I, Uetani K. Soil Dyn Earthq Eng 1999;18:363. https://doi.org/10.1016/S0267-7261(99)00007-X.
[27] Constantinou MC, Symans MD. Experimental and analytical investigation of seismic response of structures with supplemental fluid viscous dampers. Rep. No. NCEER-92-0032. Buffalo, N.Y: National Center for Earthquake Engineering Research, State University of New York at Buffalo; 1992.
[28] Hwang JS, Huang YN, Yi SL, Ho SY. J Struct Eng 2008;134:22. https://doi.org/10.1061/(ASCE)0733-9445(2008)134:1(22).
[29] Hwang JS, Lin WC, Wu NJ. Struct Infrastruct Eng 2013;9:28. https://doi.org/10.1080/15732479.2010.513713.
[30] Hanson RD, Soong TT. Seismic design with supplemental energy dissipation devices. Oakland, CA: EERI; 2001.
[31] Taylor DP, Tonawanda NY. Toggle linkage seismic isolation structure. 1999. Patent no. 5934028.
[32] Zhang R, He H, Weng D, Zhou H, Ding S. Sci Iran 2012;19:1379. https://doi.org/10.1016/j.scient.2012.10.011.
[33] Sigaher A, Constantinou MC. Earthq Spectra 2003;19:133. https://doi.org/10.1193/1.1540999.
[34] Seleemah A, Constantinou MC. Investigation of seismic response of buildings with linear and nonlinear fluid viscous dampers. 1997. Report No. NCEER 970004, Buffalo, N.Y.
[35] Gandomzadeh A. Dynamic soil-structure interaction: effect of nonlinear soil behavior. PhD thesis. University of Paris-Est; 2011. https://tel.archives-ouvertes.fr/tel-00648179.
[36] Gazetas C, Anastasopoulos I, Adamidis O, Kontoroupi Th. Soil Dyn Earthq Eng 2013;47:83. https://doi.org/10.1016/j.soildyn.2012.12.011.
[37] Bolisetti C, Whittaker AS, Coleman JL. Soil Dyn Earthq Eng 2018;107:218. https://doi.org/10.1016/j.soildyn.2018.01.026.
[38] Kausel E. Soil Dyn Earthq Eng 2010;30(9):822. https://doi.org/10.1016/j.soildyn.2009.11.001.
[39] Gazetas C. J Geotech Eng 1991;117:1363. https://doi.org/10.1061/(ASCE)0733-9410(1991)117:9(1363).
[40] Newmark NM, Hall WJ. Earthquake spectra and design. first ed. Berkeley, California: Earthquake Engineering Research Institute; 1982.
[41] Ellis BR. Proc Inst Civ Eng 1980;69:763. https://doi.org/10.1680/iicep.1980.2376.
[42] Stafford B, Coull A. Tall building structures: analysis and design. first ed. United States of America: John Wiley & Sons, INC.; 1991.
[43] Goel RK, Chopra AK. J Struct Eng 1997;123:1454. https://doi.org/10.1061/(ASCE)0733-9445(1997)123:11(1454).

[44] Goel RK, Chopra AK. J Struct Eng 1998;124:426. https://doi.org/10.1061/(ASCE)0733-9445(1998)124:4(426).
[45] Miranda E, Reyes CJ. J Struct Eng 2002;128:840. https://doi.org/10.1061/(ASCE)0733-9445(2002)128:7(840).
[46] Chopra AK. Dynamics of structures: theory and applications to earthquake engineering. third ed. New Jersey: Pearson; 2007.
[47] De Domenico D, Falsone G, Ricciardi G. Eng Struct 2018;162:198. https://doi.org/10.1016/j.engstruct.2018.02.037.
[48] De Domenico D, Ricciardi G. J Sound Vib 2019;452:169. https://doi.org/10.1016/j.jsv.2019.04.010.
[49] Liu MY, Chiang WL, Hwang JH, Chu CR. J Wind Eng Ind Aerodyn 2008;96:1092. https://doi.org/10.1016/j.jweia.2007.06.034.
[50] Singh SK, Mena E, Castro R. Bull Seismol Soc Am 1988;78:451.
[51] Anderson JG, Bodín P, Brune JN, Prince J, Singh SK, Quaas R, Onate M. Earthq Sci 1986;233:1043. https://doi.org/10.1126/science.233.4768.1043.
[52] Lermo J, Chávez-García FJ. Soil Dyn Earthq Eng 1994;13:413. https://doi.org/10.1016/0267-7261(94)90012-4.
[53] Chávez-García FJ, Ives-Bard P. Soil Dyn Earthq Eng 1994;13:229. https://doi.org/10.1016/0267-7261(94)90028-0.
[54] Ye L, Lay T, Bai Y, Cheung KF, Kanamori H. Geophys Res Lett 2017;44:11824.
[55] Mirwald A, Cruz-Atieza VM, Díaz-Mojica J, Iglesias A, Singh SK, Villafuerte C, Tago J. Geophys Res Lett 2017;46:2054. https://doi.org/10.1029/2018GL080904.
[56] Iiida M. Earthq Eng Struct Dyn 1998;27:1483. https://doi.org/10.1002/(sici)1096-9845(199812)27:12<1483::aid-eqe796>3.0.co;2-8.
[57] Arroyo D, Ordaz M, Ovando-Shelley E, Guasch JC, Lermo J, Perez C, Alcantara L, Ramírez-Centeno M. Dyn Earthq Eng 2013;44:54. https://doi.org/10.1016/j.soildyn.2012.08.009.
[58] Avilés J, Pérez-Rocha LE. Dyn Earthq Eng 2010;30:981. https://doi.org/10.1016/j.soildyn.2010.04.009.
[59] CFE. Manual de Diseño de Obras Civiles: Diseño por Viento. México: Instituto de Investigaciones Eléctricas; 2008.
[60] Castro HG, De Bortoli ME, Paz RR, Marighetti JO. Rev int métodos numér cálc diseño ing 2015;31:235. https://doi.org/10.1016/j.rimni.2014.08.001.